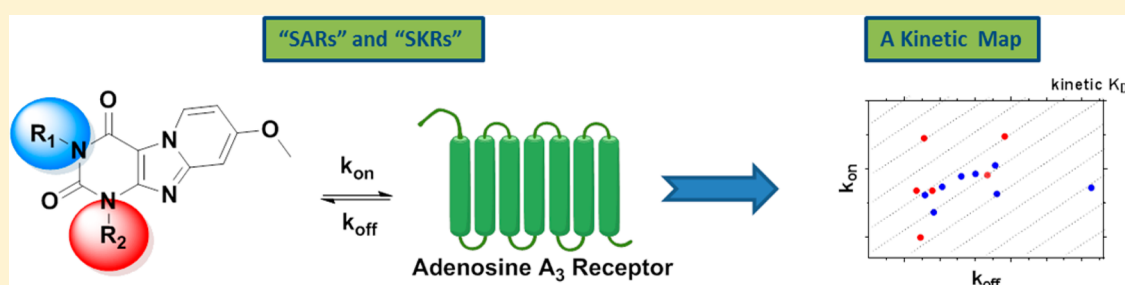


Structure–Affinity Relationships and Structure–Kinetics Relationships of Pyrido[2,1-*f*]purine-2,4-dione Derivatives as Human Adenosine A₃ Receptor Antagonists

Lizi Xia, Wessel A. C. Burger, Jacobus P. D. van Veldhoven, Boaz J. Kuiper, Tirsia T. van Duijl, Eelke B. Lenselink, Ellen Paasman, Laura H. Heitman, and Adriaan P. IJzerman*¹

Division of Medicinal Chemistry, Leiden Academic Centre for Drug Research, Leiden University, 2300 RA Leiden, The Netherlands

Supporting Information



ABSTRACT: We expanded on a series of pyrido[2,1-*f*]purine-2,4-dione derivatives as human adenosine A₃ receptor (hA₃R) antagonists to determine their kinetic profiles and affinities. Many compounds showed high affinities and a diverse range of kinetic profiles. We found hA₃R antagonists with very short residence time (RT) at the receptor (2.2 min for **5**) and much longer RTs (e.g., 376 min for **27** or 391 min for **31**). Two representative antagonists (**5** and **27**) were tested in [³⁵S]GTPγS binding assays, and their RTs appeared correlated to their (in)surmountable antagonism. From a $k_{\text{on}}-k_{\text{off}}-K_{\text{D}}$ kinetic map, we divided the antagonists into three subgroups, providing a possible direction for the further development of hA₃R antagonists. Additionally, we performed a computational modeling study that sheds light on the crucial receptor interactions, dictating the compounds' binding kinetics. Knowledge of target binding kinetics appears useful for developing and triaging new hA₃R antagonists in the early phase of drug discovery.

INTRODUCTION

The adenosine A₃ receptor is the youngest member discovered in the family of adenosine receptors,¹ all of which belong to class A G-protein coupled receptors (GPCRs) and fall into four distinct subtypes (A₁, A_{2A}, A_{2B}, and A₃). Although all subtypes are activated by the endogenous ligand adenosine, these purinergic receptors differ from each other in their distribution and to which G protein they are coupled. Following agonist activation, the A₁ and A₃ adenosine receptors cause a decrease in cAMP levels as they primarily couple to G_i proteins. The A_{2A} and A_{2B} adenosine receptors, on the other hand, are primarily linked to G_s proteins, and this leads to increased levels of cAMP upon receptor activation.²

Although the pharmacological characterization of adenosine receptors has been well documented,³ the human adenosine A₃ receptor (hA₃R) is less well characterized because of its "dichotomy" in different therapeutic applications.⁴ Moreover, certain ligands have been described as cytoprotective or cytotoxic merely depending on the concentration employed, highlighting the difficulties that arise when characterizing novel hA₃R compounds.⁵ Nevertheless, there is no doubt that the hA₃R has therapeutic potential in clinical indications (i.e., cardiovascular diseases,^{6,7} cancer,^{7,8} and respiratory dis-

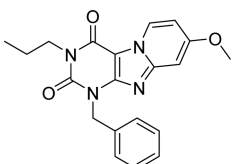
eases^{7,9–11}) due to its overexpression on cancer and inflammatory cells.^{3,12–15}

Traditional drug screening methods, and those employed in previous hA₃R drug discovery attempts, revolve around the use of a ligand's affinity as the selection criterion for further optimization in a so-called structure–affinity relationships (SAFIRs) approach. In recent years, however, there has been emerging the realization that selecting ligands based on their affinity, an equilibrium parameter, does not necessarily predict in vivo efficacy. This is due to the dynamic conditions in vivo that often are in contrast to the equilibrium conditions applied in in vitro assays.¹⁶ In fact, a ligand's kinetic properties may provide a better indication of how a ligand will perform in vivo.¹⁷ Specifically, the parameter of residence time (RT) has been proposed as a more relevant selecting criterion. The RT reflects the lifetime of the ligand–receptor complex and can be calculated as the reciprocal of the ligand's dissociation constant ($RT = 1/k_{\text{off}}$).^{18,19}

While the binding kinetics of some (labeled) hA₃R agonists have been studied,²⁰ this parameter has not been part of

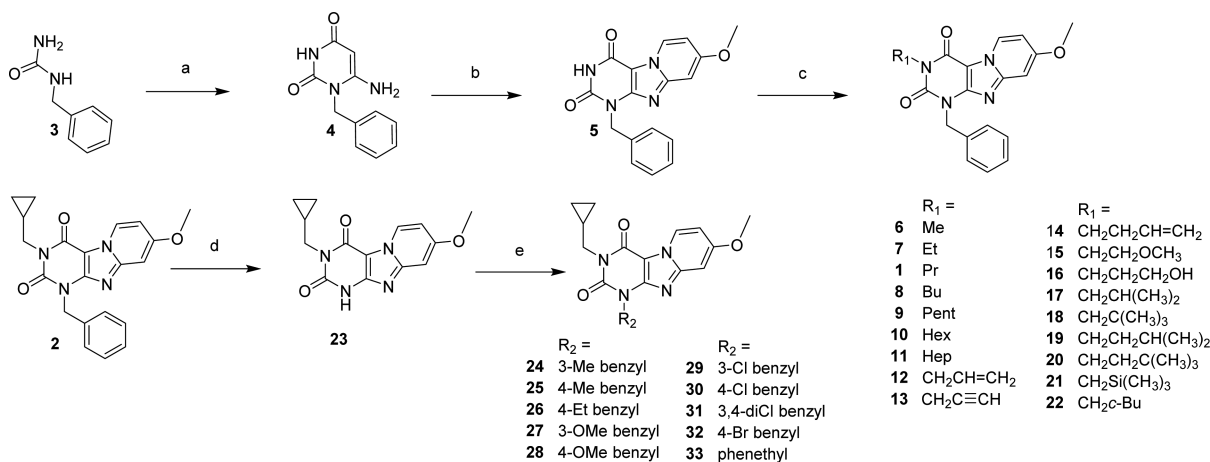
Received: June 28, 2017

Published: August 14, 2017

Table 1. Binding Affinity and Kinetic Parameters of 1-Benzyl-8-methoxy-3-propylpyrido[2,1-*f*]purine-2,4(1*H*,3*H*)-dione^{23,24}


compd	p <i>K</i> _i ^a ± SEM (mean <i>K</i> _i in nM)	KRI ^b	<i>k</i> _{on} ^c (M ⁻¹ s ⁻¹)	<i>k</i> _{off} ^d (s ⁻¹)	RT ^e (min)
1	8.5 ± 0.02 (3.2)	0.99 (0.97, 1.0)	(8.5 ± 1.2) × 10 ⁵	(3.2 ± 0.02) × 10 ⁻⁴	52 ± 0.3

^ap*K*_i ± SEM (*n* ≥ 3, average *K*_i value in nM), obtained at 25 °C from radioligand binding assays with [³H]34 on human adenosine A₃ receptors stably expressed on CHO cell membranes. ^bKRI (*n* = 2, individual estimates in parentheses), obtained at 10 °C from dual-point competition association assays with [³H]34 on human adenosine A₃ receptors stably expressed on CHO cell membranes. ^c*k*_{on} ± SEM (*n* ≥ 3), obtained at 10 °C from competition association assays with [³H]34 on human adenosine A₃ receptors stably expressed on CHO cell membranes. ^d*k*_{off} ± SEM (*n* ≥ 3), obtained at 10 °C from competition association assays with [³H]34 on human adenosine A₃ receptors stably expressed on CHO cell membranes. ^eRT (min) = 1/(60 × *k*_{off}).

Scheme 1. Synthesis of 1,3-Disubstituted-1*H*,3*H*-pyrido[2,1-*f*]purine-2,4-dione Derivatives^a

^a(a) ethyl cyanoacetate, NaOEt, EtOH, reflux, overnight; (b) (i) NBS, CH₃CN, 80 °C, 1 h, (ii) 4-methoxypyridine, 80 °C, overnight; (c) R₁-Br, DBU, CH₃CN, 80 °C, overnight; (d) 20% Pd(OH)₂, ammonium formate, EtOH, reflux, overnight; (e) R₂-Br, K₂CO₃, DMF, 40 °C, overnight.

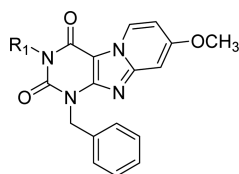
medicinal chemistry efforts for antagonists, i.e., yielding structure–kinetics relationships (SKRs), next to SAFIRs.²¹ Therefore, to provide the first SKR analysis on the hA₃R, a highly potent and selective hA₃R antagonist scaffold was chosen. The pyrido[2,1-*f*]purine-2,4-dione template has been previously characterized with respect to affinity alone. In a Topliss approach,²² we had synthesized and characterized a number of highly potent and selective hA₃R antagonists.^{23,24} One of the reference antagonists (1) with good affinity and selectivity over other adenosine receptors is represented in Table 1. Using this compound as the starting point, we further selected and synthesized compounds to add to the library of pyrido[2,1-*f*]purine-2,4-dione derivatives. Using radioligand displacement assays and competition association assays, we obtained affinity (*K*_i) and kinetic parameters (*k*_{on}, *k*_{off} and RTs). This allowed a full SKR study alongside a more traditional SAFIR analysis. The findings provide information on the structural requirements for a favorable kinetic profile at the hA₃R and consequently may improve the in vitro to in vivo translation for hA₃R antagonists.

RESULTS AND DISCUSSION

Chemistry. The synthesis approach shown in Scheme 1 was adapted from Priego et al.^{23,24} Starting from the commercially available materials benzylurea (3), ethyl cyanoacetate, and sodium methoxide. 1-benzyl-6-amino-uracil (4) was synthe-

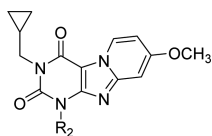
sized in an 88% yield.²⁵ In situ dibromination of uracil 4 at the C⁵ position by *N*-bromosuccinimide, followed by cyclization with 4-methoxypyridine, gave the pyrido[2,1-*f*]purine-2,4-dione (5) in a one-pot reaction. Final compounds 1, 2, and 6–22 (as depicted in Table 1) were obtained, with yields varying in the range of 3–86%, by alkylating the N³ position of 5 using a variety of alkyl, alkenyl, and alkynyl bromides in acetonitrile and 1,8-diazabicyclo[5.4.0]undec-7-ene (DBU) as a base. Second, to be able to diversify on the N¹ (R₂) position, building block 23 had to be obtained. Full conversion of methylcyclopropyl compound 2 into the desired debenzylated 23 was realized by multiple additions of ammonium formate and Pd(OH)₂ at 80 °C in ethanol overnight. Because of poor solubility, 23 was extracted with hot DMF and Pd(OH)₂ was removed by filtration, resulting in a quantitative yield. Finally, various N¹ substituted benzyl (24–32) and phenethyl (33) derivatives (Scheme 1) were made starting from the respective benzyl- or phenethyl bromides in DMF with K₂CO₃ used as base.

Biological Evaluation. All binding affinities of the pyrido[2,1-*f*]purine-2,4-dione derivatives were determined at 25 °C in a 2 h incubation protocol. All compounds were able to concentration-dependently inhibit specific [³H]8-ethyl-4-methyl-2-phenyl-(8*R*)-4,5,7,8-tetrahydro-1*H*-imidazo[2,1-*i*]purin-5-one²⁶ ([³H]PSB-11, 34) binding to the human adenosine A₃ receptor, and their affinities are listed in Tables 1, 2 and 3.

Table 2. Binding Affinities and Kinetic Parameters of Pyrido[2,1-*f*]purine-2,4-dione Derivatives with Modification on N-3 Position (R₁ Group)

compd	R ₁	pK _i ^a ± SEM (mean K _i in nM)	KRI ^b	k _{on} ^c (M ⁻¹ s ⁻¹)	k _{off} ^d (s ⁻¹)	RT ^e (min)
5	H	7.0 ± 0.02 (108)	0.38 ± 0.12	(5.3 ± 1.5) × 10 ⁵	(1.4 ± 0.5) × 10 ⁻²	2.2 ± 1.4
6	CH ₃	7.7 ± 0.1 (20.8)	0.54 (0.52, 0.55)	nd ^f	nd	nd
7	CH ₂ CH ₃	8.0 ± 0.1 (10.7)	0.80 (0.85, 0.75)	nd	nd	nd
8	CH ₂ CH ₂ CH ₂ CH ₃	8.8 ± 0.1 (1.5)	1.29 (1.27, 1.31)	nd	nd	nd
9	CH ₂ CH ₂ CH ₂ CH ₂ CH ₃	8.5 ± 0.02 (3.5)	1.11 (0.98, 1.24)	(1.1 ± 0.1) × 10 ⁶	(6.0 ± 0.5) × 10 ⁻⁴	28 ± 2.2
10	CH ₂ CH ₂ CH ₂ CH ₂ CH ₂ CH ₃	8.6 ± 0.1 (2.8)	2.18 (2.15, 2.21)	(2.3 ± 1.0) × 10 ⁵	(8.2 ± 1.3) × 10 ⁻⁵	213 ± 35
11	CH ₂ CH ₂ CH ₂ CH ₂ CH ₂ CH ₂ CH ₃	8.2 ± 0.2 (6.8)	4.06 (3.66, 4.46)	(4.2 ± 0.3) × 10 ⁵	(6.2 ± 0.2) × 10 ⁻⁵	278 ± 45
12	CH ₂ CH=CH ₂	8.3 ± 0.1 (5.9)	0.72 (0.46, 0.99)	nd	nd	nd
13	CH ₂ C≡CH	8.4 ± 0.02 (4.3)	1.20 (1.16, 1.23)	nd	nd	nd
14	CH ₂ CH ₂ CH=CH ₂	8.9 ± 0.1 (1.4)	1.23 (1.04, 1.41)	nd	nd	nd
15	CH ₂ CH ₂ OCH ₃	7.7 ± 0.2 (23)	0.70 (0.70, 0.70)	(4.3 ± 0.8) × 10 ⁵	(6.3 ± 0.7) × 10 ⁻⁴	27 ± 2.6
16	CH ₂ CH ₂ CH ₂ OH	7.1 ± 0.1 (81)	1.04 ± 0.11	nd	nd	nd
17	CH ₂ CH(CH ₃) ₂	8.9 ± 0.02 (1.2)	1.64 ± 0.24	(7.8 ± 2.7) × 10 ⁵	(2.0 ± 0.8) × 10 ⁻⁴	148 ± 102
18	CH ₂ C(CH ₃) ₃	8.5 ± 0.1 (3.5)	1.73 ± 0.28	(5.5 ± 1.3) × 10 ⁵	(1.1 ± 0.4) × 10 ⁻⁴	250 ± 147
19	CH ₂ CH ₂ CH(CH ₃) ₂	8.5 ± 0.04 (3.5)	1.39 (1.23, 1.55)	nd	nd	nd
20	CH ₂ CH ₂ C(CH ₃) ₃	8.1 ± 0.02 (8.0)	0.95 (1.02, 0.87)	nd	nd	nd
21	CH ₂ Si(CH ₃) ₃	8.6 ± 0.03 (2.7)	1.36 (1.26, 1.45)	nd	nd	nd
2	CH ₂ C ₃ H ₅	9.0 ± 0.02 (1.0)	2.68 ± 0.48	(2.8 ± 0.5) × 10 ⁶	(6.0 ± 1.7) × 10 ⁻⁵	315 ± 105
22	CH ₂ C ₄ H ₇	8.6 ± 0.03 (2.7)	1.48 (1.66, 1.30)	nd	nd	nd

^apK_i ± SEM (*n* ≥ 3, average K_i value in nM), obtained at 25 °C from radioligand binding assays with [³H]34 on human adenosine A₃ receptors stably expressed on CHO cell membranes. ^bKRI ± SEM (*n* = 3) or KRI (*n* = 2, individual estimates in parentheses), obtained at 10 °C from dual-point competition association assays with [³H]34 on human adenosine A₃ receptors stably expressed on CHO cell membranes. ^ck_{on} ± SEM (*n* ≥ 3), obtained at 10 °C from competition association assays with [³H]34 on human adenosine A₃ receptors stably expressed on CHO cell membranes. ^dk_{off} ± SEM (*n* ≥ 3), obtained at 10 °C from competition association assays with [³H]34 on human adenosine A₃ receptors stably expressed on CHO cell membranes. ^eRT (min) = 1/(60 × k_{off}). ^fnd = not determined.

Table 3. Binding Affinities and Kinetic Parameters of Pyrido[2,1-*f*]purine-2,4-dione Derivatives with Modification at R₂

compd	R ₂	pK _i ^a ± SEM (mean K _i in nM)	KRI ^b	k _{on} ^c (M ⁻¹ s ⁻¹)	k _{off} ^d (s ⁻¹)	RT ^e (min)
2	benzyl	9.0 ± 0.02 (1.0)	2.68 ± 0.48	(2.8 ± 0.5) × 10 ⁶	(6.0 ± 1.7) × 10 ⁻⁵	315 ± 105
24	3-CH ₃ -benzyl	8.8 ± 0.02 (1.5)	1.18 (1.18, 1.17)	nd ^f	nd	nd
25	4-CH ₃ -benzyl	9.0 ± 0.1 (0.92)	1.15 (1.03, 1.27)	nd	nd	nd
26	4-CH ₂ CH ₃ -benzyl	9.2 ± 0.04 (0.71)	0.81 (0.82, 0.79)	nd	nd	nd
27	3-OCH ₃ -benzyl	9.4 ± 0.03 (0.38)	2.24 (2.32, 2.15)	(4.8 ± 0.2) × 10 ⁵	(4.7 ± 0.7) × 10 ⁻⁵	376 ± 58
28	4-OCH ₃ -benzyl	8.9 ± 0.01 (1.4)	1.39 (1.22, 1.55)	(4.8 ± 0.1) × 10 ⁵	(7.8 ± 2.0) × 10 ⁻⁵	250 ± 72
29	3-Cl-benzyl	8.3 ± 0.02 (4.9)	0.89 (1.06, 0.72)	(8.2 ± 1.3) × 10 ⁵	(4.7 ± 0.7) × 10 ⁻⁴	36 ± 5.5
30	4-Cl-benzyl	8.9 ± 0.01 (1.2)	1.11 (1.02, 1.20)	(3.0 ± 0.3) × 10 ⁶	(8.2 ± 0.2) × 10 ⁻⁴	20 ± 0.5
31	3,4-dichlorobenzyl	8.3 ± 0.01 (5.3)	3.12 (3.49, 2.75)	(1.0 ± 0.1) × 10 ⁵	(5.3 ± 1.5) × 10 ⁻⁵	391 ± 137
32	4-Br-benzyl	8.9 ± 0.1 (1.2)	1.19 (1.30, 1.08)	nd	nd	nd
33	phenethyl	8.1 ± 0.04 (7.7)	1.09 (1.21, 0.97)	nd	nd	nd

^apK_i ± SEM (*n* ≥ 3, average K_i value in nM), obtained at 25 °C from radioligand binding assays with [³H]34 on human adenosine A₃ receptors stably expressed on CHO cell membranes. ^bKRI ± SEM (*n* = 3) or KRI (*n* = 2, individual estimates in parentheses), obtained at 10 °C from dual-point competition association assays with [³H]34 on human adenosine A₃ receptors stably expressed on CHO cell membranes. ^ck_{on} ± SEM (*n* ≥ 3), obtained at 10 °C from competition association assays with [³H]34 on human adenosine A₃ receptors stably expressed on CHO cell membranes. ^dk_{off} ± SEM (*n* ≥ 3), obtained at 10 °C from competition association assays with [³H]34 on human adenosine A₃ receptors stably expressed on CHO cell membranes. ^eRT (min) = 1/(60 × k_{off}). ^fnd = not determined.

All compounds had (sub)nanomolar binding affinities ranging from 0.38 nM for compound 27 to 108 nM for compound 5.

Subsequently, the human adenosine A₃ receptor ligands were screened in a so-called “dual-point” competition association

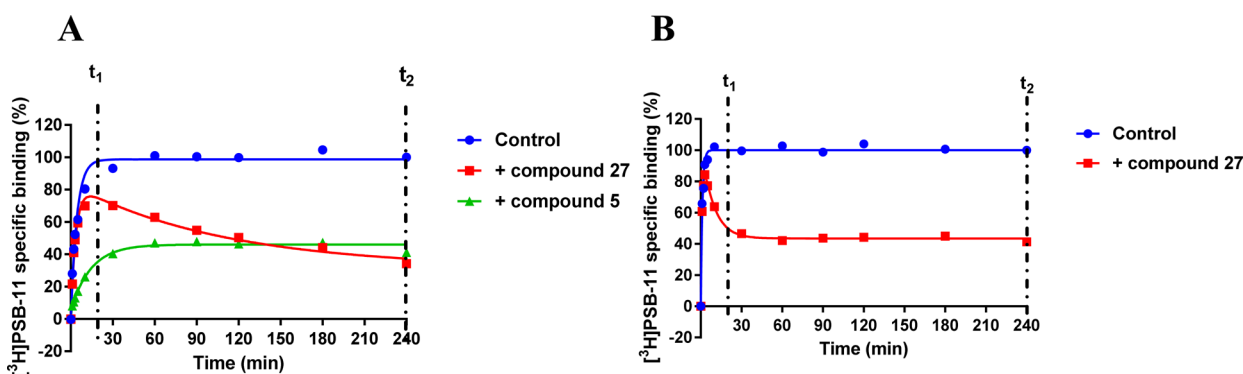


Figure 1. (A) Representative competition association assay curves of [^3H]34 in the absence (control) or presence of a long residence time compound 27 and a short residence time compound 5. Experiments were performed at 10 °C using the compound's respective IC_{50} value at the hA_3R . (B) Competition association curves of [^3H]34 in the absence (control) or presence of long residence time compound 27. Experiments were performed at 25 °C using the compound's respective IC_{50} value at the hA_3R . t_1 is the radioligand binding at 20 min, while t_2 is the radioligand binding at 240 min.

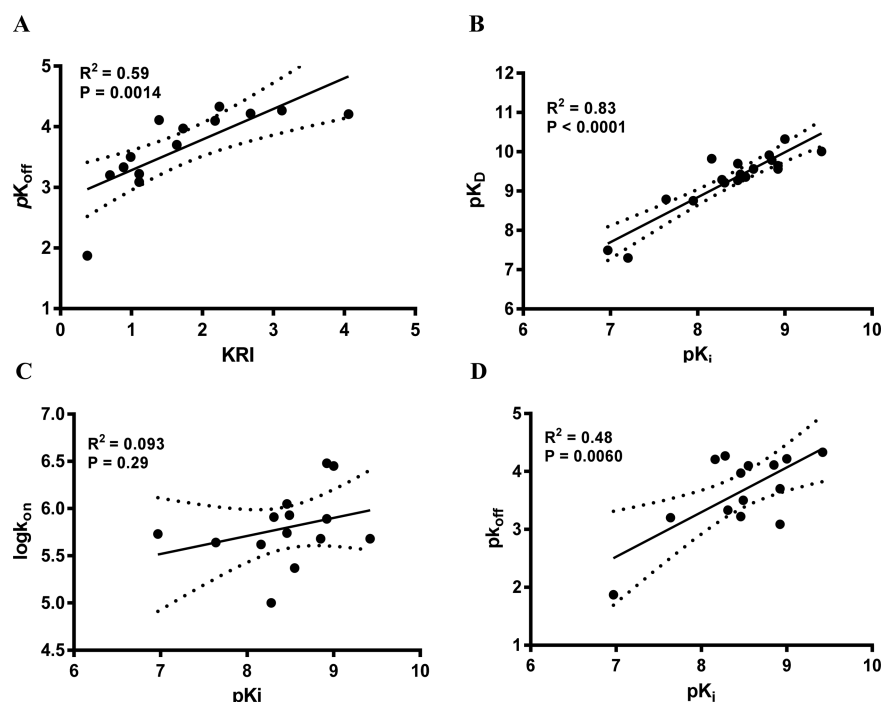


Figure 2. Correlations between the negative logarithm of the human adenosine A_3 receptor antagonists' dissociation rates (pK_{off}) and their kinetic rate index (KRI) (A), the human adenosine A_3 receptor antagonists' affinity (pK_i) and their "kinetic K_D " (pK_D) (B), association rate constants ($\log k_{\text{on}}$) (C), and dissociation rate constants (pK_{off}) (D). The central line corresponds to the linear regression of the data, the dotted lines represent the 95% confidence intervals for the regression. Data used in these plots are detailed in Tables 1–3. Data are expressed as mean from at least three independent experiments.

assay,²⁷ allowing for the semiquantitative estimation of the compounds' dissociation rates and therefore the compounds' RTs. The specific binding of [^3H]34 was measured after 20 and 240 min in the absence and presence of a single concentration (i.e., $1 \times \text{IC}_{50}$) of unlabeled human adenosine A_3 receptor antagonists, which yielded their kinetic rate index (KRI). A long RT compound shows a characteristic "overshoot" followed by a steady decrease in specific binding until a new equilibrium is reached; in such a case, the KRI value is greater than unity. Conversely, a ligand with a fast dissociation rate is represented by a more shallow curve, yielding a KRI value smaller than one when dividing the binding at t_1 by the binding at t_2 . The KRI values in the series ranged from 0.38 to 4.06 (Table 1, 2, and 3).

Compounds with a KRI value less than 0.7 or greater than 1.5 were selected for complete kinetic characterization through the use of a competition association assay with [^3H]34 (Figure 1A). To obtain extensive structure–kinetics relationships (SKRs), close structural analogues (9, 28, 29, and 30) of 1 were also tested to obtain their association (k_{on}) and dissociation (k_{off}) rate constants. Association rate constants varied by 30-fold, ranging from $(1.0 \pm 0.1) \times 10^5 \text{ M}^{-1} \text{ s}^{-1}$ for antagonist 31 to $(3.0 \pm 0.3) \times 10^6 \text{ M}^{-1} \text{ s}^{-1}$ for antagonist 30 (Table 3). Interestingly, there was an approximately 290-fold difference in dissociation rate constants, reflecting the divergent KRI values. Antagonist 5 had the fastest dissociation rate constant of $(1.4 \pm 0.5) \times 10^{-2} \text{ s}^{-1}$ and thus the shortest RT of 2.2 min, while both antagonist 27 and 31 had the slowest

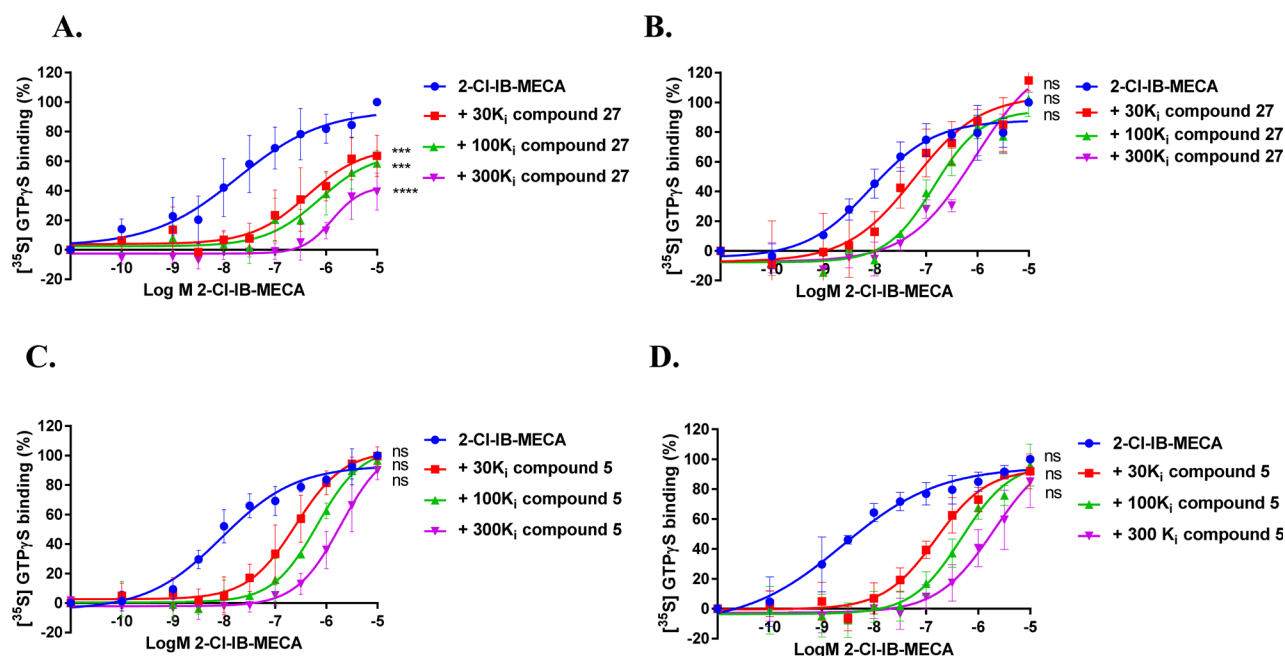


Figure 3. 2-Cl-IB-MECA-stimulated [^{35}S] GTP γ S binding to hA $_3$ R stably expressed on CHO cell membranes (25 °C) in the absence or presence of long-residence-time antagonist 27 (A and B, normalized and combined, $n \geq 3$) or short-residence-time antagonist 5 (C and D, normalized and combined, $n \geq 3$). Antagonist 27 (A) and 5 (C) were incubated for 60 min prior to the challenge of the hA $_3$ R agonist 2-Cl-IB-MECA, at a concentration ranging from 0.1 nM to 10 μM , for another 30 min. Antagonist 27 (B) and 5 (D) were coincubated with 2-Cl-IB-MECA, at the same concentration range, for 30 min. The agonist curves were generated in the presence of increasing concentrations of antagonists, namely 30-, 100-, and 300-fold their respective K_i values. Curves were fitted to a four parameter logistic dose–response equation. Data is from at least three independent experiments performed in duplicate, normalized according to the maximal response (100%) produced by 2-Cl-IB-MECA alone. The shift in agonist EC_{50} values was determined to perform Schild analyses. Two-way ANOVA with Dunnett’s post-test was applied for the comparison of E_{max} by agonist control, * $p < 0.05$, ** $p < 0.01$, *** $p < 0.001$, **** $p < 0.0001$, ***** $p < 0.00001$, ns for not significant.

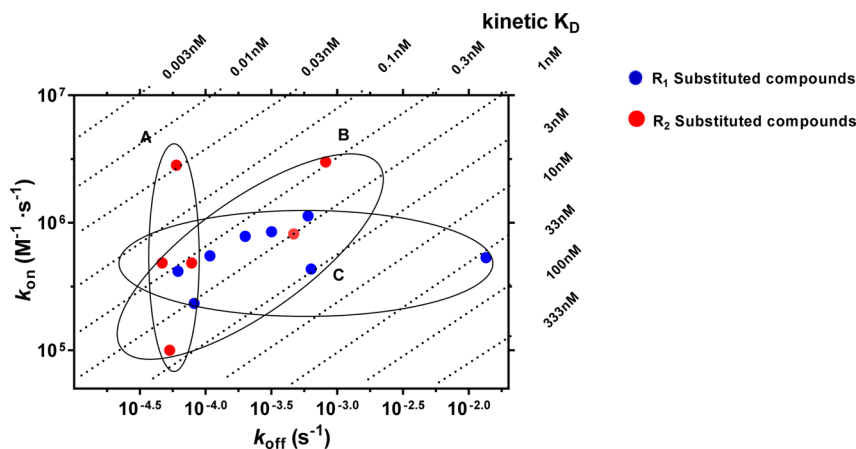


Figure 4. Kinetic map (y axis, k_{on} in $\text{M}^{-1} \text{s}^{-1}$; x axis, k_{off} in s^{-1}) of all compounds that were kinetically characterized in this study. k_{on} and k_{off} values were obtained through competition association assays performed at the hA $_3$ R. The kinetically derived affinity ($K_D = k_{\text{off}}/k_{\text{on}}$) is represented through diagonal parallel lines. Group A: compounds that show similar k_{off} values but due to differing k_{on} values have different K_D values. Group B: compounds that display similar K_D values despite showing divergent k_{off} and k_{on} values. Group C: compounds with similar k_{on} values, but due to differing k_{off} values have different K_D values.

dissociation rate constants of $(4.7 \pm 0.7) \times 10^{-5} \text{ s}^{-1}$ and $(5.3 \pm 1.5) \times 10^{-5} \text{ s}^{-1}$, respectively, and thus the longest RTs of 376 and 391 min, respectively. Notably, the long RT antagonist 27 (Figure 1A) displayed a typical “overshoot” in the competition association curve, indicative of a slower dissociation than the radiolabeled probe [^3H]34, while the short RT antagonists, exemplified by antagonist 5 (Figure 1A), presented more shallow, gradually ascending curves. There was a good correlation between the negative logarithm of the antagonists’

dissociation rate constants and their KRI values derived from the kinetic screen (Figure 2A), which confirmed that a compound’s KRI value is a good predictor for its dissociation rate constant. Notably, the experimental temperatures in the kinetic assays were lower than in the equilibrium displacement assays (25 °C vs 10 °C) because kinetic studies performed at 25 °C were compromised by the nature of the compounds tested. This is shown in Figure 1B, where the “overshoot” of long RT antagonist 27 happened before the t_1 checkpoint of 20 min,

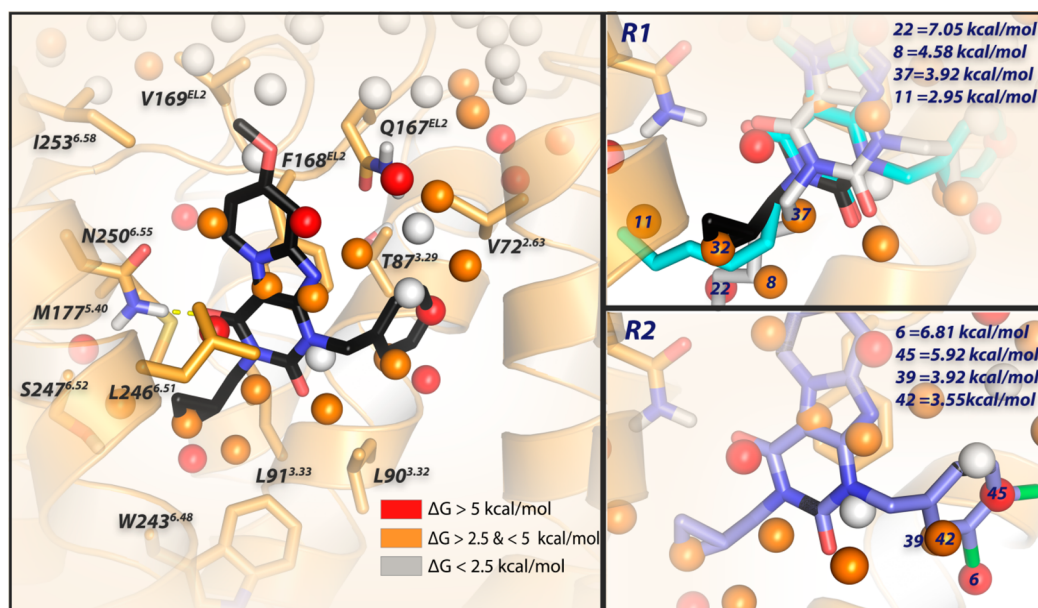


Figure 5. Docking of antagonist **2** into the binding site of the homology model of the adenosine A_3 receptor based on the crystal structure of the adenosine A_{2A} receptor (PDB 4E1Y).⁴¹ Antagonist **2** is represented by black sticks, and residues within 5 Å of **2** are visualized as orange sticks. The protein is represented by orange ribbons. Ligand and residues atoms color code: red = oxygen, blue = nitrogen, white = hydrogen. The overlay of consecutively numbered hydration sites (colored spheres; for color code, see below) were calculated by WaterMap (left). Hydration sites shown as red and orange spheres represent positions where “unstable” water molecules can be found, which should be displaced by antagonist **2**. White spheres symbolize “stable” water molecules, which are in exchange with the bulk solvent. Two different binding modes are represented for antagonist **10** (cyan and gray sticks), which shows that the flexible hexyl chain can displace different hydration sites (8 for gray and 11 for cyan). For the key hydration sites (8, 11, 22, 32, 37) surrounding the lipophilic “tails”, calculated ΔG values (in kcal/mol) with respect to bulk solvent are shown (upper right). Hydration sites 6, 39, 42, and 45 are proposed to be displaced by the 3,4 dichloro substituents of **31**; calculated ΔG values (in kcal/mol) with respect to bulk solvent are shown (lower right).

which did not happen at 10 °C. A significant correlation was also observed between the antagonist affinities (K_i values) determined in equilibrium displacement experiments and their kinetic K_D values derived from competition association experiments (Figure 2B), despite the differences in assay temperature (25 °C vs 10 °C). Interestingly, the kinetic association rate constants (k_{on}) did not show any significant correlation with affinity (Figure 2C), while the dissociation rate constants (k_{off}) had a fair correlation with affinity (Figure 2D).

The representative long RT and short RT antagonists (**27** and **5**) were selective for the hA_3 receptor when compared to other adenosine receptors (i.e., human adenosine A_1 and A_{2A} receptor, Supporting Information, Table S1). These two antagonists (**27** and **5**) with comparable association rate constants but distinct dissociation rate constants (or RTs) were further analyzed in a [³⁵S]GTP γ S binding assay in which we studied the (in)surmountable antagonism induced by the two compounds (Figure 3). Moreover, a k_{on} – k_{off} – K_D “kinetic map” (Figure 4) was constructed based on the compounds’ divergent affinities (expressed as kinetic K_D values) and kinetics parameters, yielding a division of these antagonists into three different subcategories: antagonists that show similar k_{off} values (<2-fold) but due to differing k_{on} values (>28-fold) have different K_D values (~100-fold, group A), antagonists that display similar K_D values (<10-fold) despite showing divergent k_{off} and k_{on} values (17-fold and 30-fold, group B), and antagonists with similar k_{on} values (<5-fold) but due to differing k_{off} values (~290-fold) have different K_D values (>110-fold, group C). Additionally, we applied molecular modeling to compare the binding behavior in some molecular detail of

several antagonists with similar affinities (**2** vs **10**; **31** vs **29** or **30**) (Figure 5).

Structure–Affinity Relationships (SAFIRs) and Structure–Kinetics Relationships (SKRs). According to previous studies from our group,^{23,24} methoxy-substitution at the C⁸ position (Table 1) of the pyrido[2,1-*f*]purine-2,4-dione scaffold yielded selective hA_3R antagonists with good affinity (3.2 nM for **1** as a reference compound). From our preliminary studies, this methoxy-group appeared important for slow dissociation (**1** vs compound **S2** from Supporting Information, Figure S1, Table S2). Because of the nanomolar affinity and close-to-unity KRI value of **1**, it was treated as the starting point of this SAFIR and SKR study, having, on further analysis, an association rate constant of $(8.5 \pm 1.2) \times 10^5 \text{ M}^{-1} \text{ s}^{-1}$ and a dissociation rate constant of $(3.2 \pm 0.02) \times 10^{-4} \text{ s}^{-1}$ (RT = 52 min). Next, we decided to investigate R_1 substitutions (Table 2), beginning with antagonist **5** ($R_1 = \text{H}$).

The Substitutions at R_1 (Table 2). First, an increase in alkyl chain length was investigated, indicating an elongated carbon chain had a cumulative effect on KRI (**5**, **6**, **7**, **8**, **10**, **11**), with the exception of antagonist **9** (KRI values from 0.38 to 4.06). One could point to a possible correlation between lipophilicities and dissociation rate constants (and consequently RTs) to explain this trend (Supporting Information, Figure S2A). However, with all of the antagonists kinetically characterized, no such correlation was observed (Supporting Information, Figure S2B). Therefore, other reasons should be taken into account as to why elongating the carbon chain has such a profound effect on the ligand’s dissociation rate. The role of membrane–drug interactions in determining the pharmacological profile is a possible reason, especially the

role long carbon tails have in such interactions.²⁸ It is interesting to point out that the affinity of antagonist **11**, which had a traditional lead selection process taken place, would most likely have resulted in the elimination of this compound due to the more favorable affinity and hydrophilic properties of its shorter carbon chain counterparts (**8** or **9**) (affinities, 6.8 nM vs 1.5 nM or 3.5 nM; KRI values, 4.06 vs 1.29 or 1.11). This would have overlooked the efficacy this compound could offer due to its longer residence time.

Second, the presence of a more rigid substitution of the R₁ group of saturated equivalents (antagonists **1** and **8**) led to antagonists **12** and **14**, with similar improvement in the affinity pairs (**12** and **14**, 5.9 and 1.4 nM; **1** and **8**, 3.2 and 1.5 nM) and KRI values (**12** and **14**, 0.72 and 1.23; **1** and **8**, 0.99 and 1.29). Further rigidification with alkyne (**13**) rather than alkene (**12**) maintained affinities (4.3 vs 5.9 nM) and increased KRI values (1.20 vs 0.72). This alkyne could be the starting point for a further study on “click-chemistry” for introducing, e.g., fluorescent tags.^{29–31}

Third, the introduction of a polar atom or group in antagonist **15** or **16**, respectively, led to a decrease in affinity compared to their nonpolar counterpart **1** (23 or 81 nM vs 3.2 nM). The changes in KRI values between antagonist **1** and its polar counterparts **15** and **16** can be considered minor (0.99 vs 0.70 and 1.04). Of note, by comparing affinities and kinetic profiles of polar antagonist **15** with its nonpolar equivalent **1**, we found the polarity at the “lipophilic carbon chain” resulted in slower association (k_{on} of $(4.3 \pm 0.8) \times 10^5 \text{ M}^{-1} \text{ s}^{-1}$ vs $(8.5 \pm 1.2) \times 10^5 \text{ M}^{-1} \text{ s}^{-1}$) but faster dissociation (k_{off} of $(6.3 \pm 0.7) \times 10^{-4} \text{ s}^{-1}$ vs $(3.2 \pm 0.02) \times 10^{-4} \text{ s}^{-1}$), with a concomitant decrease in affinity (23 vs 3.2 nM).

Moreover, the bulkiness of the substituents was studied with branched carbon side chains (**17**, **18**, **19**, **20**, and **21**) or aliphatic rings (**2** and **22**). As to the branched carbon side chains, compound affinities remained in the nanomolar range, while in terms of KRI values, 2-carbon-linker branched side chains (**17** and **18**) caused larger KRI values than those of either their linear counterparts (**8** and **9**) or 3-carbon-linear branched side chains (**19** and **20**) (**17**, 1.64 vs 1.29 or 1.39; **18**, 1.73 vs 1.11 or 0.95). Although the association rate constants of **17** and **18** were similar to other antagonists in Table 2, the dissociation rate constants suggest their branched side chains have an extra “anchoring” effect compared with the linear counterparts. For example, the k_{off} of **18** with a 5-carbon branched side chain was quite similar to **10** or **11**, having a 6 or 7-carbon linear side chain ($(1.1 \pm 0.4) \times 10^{-4} \text{ s}^{-1}$ vs $(8.2 \pm 1.3) \times 10^{-5} \text{ s}^{-1}$ or $(6.2 \pm 0.2) \times 10^{-5} \text{ s}^{-1}$). The presence of a slightly less polar but larger silicon atom (**21**) instead of carbon (**18**) made the KRI value decrease (1.36 vs 1.73), although the affinity remained virtually the same (2.7 vs 3.5 nM).

Interestingly, another reported analogue (**2**)²³ of compound **1**, with cyclopropylmethyl substitution at the R₁ group, led to unique kinetic parameters, i.e., a combination of a fast association rate constant ($(2.8 \pm 0.5) \times 10^6 \text{ M}^{-1} \text{ s}^{-1}$ vs $(8.5 \pm 1.2) \times 10^5 \text{ M}^{-1} \text{ s}^{-1}$) and a slow dissociation rate constant ($(6.0 \pm 1.7) \times 10^{-5} \text{ s}^{-1}$ vs $(3.2 \pm 0.02) \times 10^{-4} \text{ s}^{-1}$), although the affinities of **2** and **1** were similar (1.0 ± 0.03 nM vs 3.2 ± 0.1 nM, respectively). The RT of compound **2** was the longest in Table 2 with 315 min. For the antagonist with cyclobutylmethyl (**22**), affinity (2.7 vs 1.0 nM) and KRI value (1.48 vs 2.68) were lower than for compound **2**.

Although the dissociation rate constants of the antagonists in Table 2 varied greatly depending on the R₁ substituent, the

association rate constants were more similar (within 5-fold). Association rate constants are often reasoned to be caused by a diffusion limited process whereby the collision rate of ligand and receptor determines the rate of ligand–receptor complex formation.³² When no conformational changes are required for the receptor and ligand to bind and when taking into account the proportion of the receptor responsible for binding, this sets the association rate constant at observed limits of around $10^7 \text{ M}^{-1} \text{ s}^{-1}$.³³ As the association rate constants for all R₁ substituted compounds were slower than the diffusion limit by at least 3.5 fold (**2**), we hypothesize target engagement for R₁ substituted antagonists is more hampered than imposed by the diffusion limit.

The Substitutions at R₂ Group (Table 3). From Table 2, we learned that cyclopropylmethyl-substituted antagonist **2** exhibited a kinetic profile as a long RT compound while showing the affinity previously reported.²³ As a result, this compound became the starting point for our exploration of the substitutions (R₂ group) on the aromatic ring.

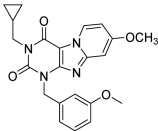
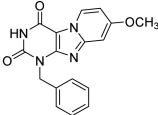
Introduction of a nonpolar alkyl substituent on antagonist **2**'s benzyl ring (**24**, **25**, **26**), resulted in a decrease in KRI values (from 2.68 to 0.81), while slight variations in affinity were observed.

Then, introduction of a polar methoxy substituent on antagonist **2**'s benzyl ring led to mixed results with a small decrease in RT at *para*-position and a slight increase in RT at *meta*-position in **28** (250 vs 315 min) and **27** (376 vs 315 min), respectively. In particular, the long residence time for **27** in combination with its subnanomolar affinity (0.38 nM) made this compound stand out in the series.

Next, halogen substitutions on antagonist **2**'s benzyl ring were examined. Apparently, the position of halogen substitution is important for affinity as *para*-substitution in antagonist **30** and **32** yielded similar affinity compared to **2** (1.2 vs 1.2 vs 1.0 nM). The one compound with *meta*-substitution, **29**, showed a 5-fold decrease in affinity compared to **2** (4.9 vs 1.0 nM). Dichloro-substituted compound **31** had the largest KRI value (3.12) among the halogen-substituted antagonists; the *para*-bromo substituted compound **32** was similar in this respect to *para*-chloro substituted **30** (1.19 vs 1.11). In a full competition association experiment, we determined the rate constants for **31** and learned it had the longest RT of all compounds kinetically characterized (391 min), concomitant with the slowest association rate constant of the compounds kinetically characterized ($(1.0 \pm 0.1) \times 10^5 \text{ M}^{-1} \text{ s}^{-1}$). Previous theoretical studies have indicated the strength of halogen bonding can be increased through the introduction of electron withdrawing groups onto halobenzenes.³⁴ Such would be the case for **31**, where the additional chloro substituent forms a stronger halogen bonding interaction with the R₂ binding pocket. Introducing a phenethyl (**33**) rather than benzyl substituent (**2**) led to a decrease in affinity (7.7 vs 1.0 nM), while the KRI value was also strongly affected (1.09 vs 2.68). This observation parallels our previous findings that the binding pocket for the R₂ substituent is of limited size.²³

Functional Assay. Following kinetic characterization, a long (**27**) and a short (**5**) RT compound were chosen for functional characterization in a [³⁵S]GTPγS binding assay, also because for these two compounds the k_{on} values were similar ($(4.8 \pm 0.2) \times 10^5 \text{ M}^{-1} \text{ s}^{-1}$ vs $(5.3 \pm 1.5) \times 10^5 \text{ M}^{-1} \text{ s}^{-1}$). This difference allowed a possible link to be made between RTs and efficacies. Pretreatment of hA₃ receptor membranes with increasing concentrations of the long RT antagonist **27**, before

Table 4. Functional Activity of hA₃ Receptor Antagonists from [³⁵S]GTPγS Binding Assays

Ligands	Preincubation		Coincubation		Mode of antagonism	
	RT ^a (min)	pA ₂ ^b	Schild slope ^b	pA ₂ ^b		Schild slope ^b
 27	376 ± 58	N.A. ^c	N.A.	8.9 ± 0.3	0.9 ± 0.2	Competitive insurmountability
 5	2.2 ± 1.4	6.8 ± 0.4	1.0 ± 0.3	7.2 ± 0.4	1.0 ± 0.2	Competitive surmountability

^aRTs were obtained from Tables 1 and 2. ^bObtained from Schild analyses. ^cN.A.: not applicable.

stimulation by the A₃ receptor agonist 2-Cl-IB-MECA, induced insurmountable antagonism. In other words, the 2-Cl-IB-MECA concentration–effect curves were shifted to the right with a concomitant decrease in the maximal response (Figure 3A). Conversely, the short RT antagonist 5 displayed surmountable antagonism, shifting 2-Cl-IB-MECA's curves to the right without affecting its maximum effect (Figure 3B). In this experimental setup, the Schild-slope of 5 generated from Schild-plots was close to unity (Table 4), and the compound's pA₂ value was comparable with its pK_i value (6.8 ± 0.4 vs 7.0 ± 0.02). We also performed coincubation experiments with these antagonists in the presence of 2-Cl-IB-MECA. In this experimental setup, all antagonists produced a rightward shift of the 2-Cl-IB-MECA concentration–effect curves without a suppression of the maximal response (Figure 3C,D). Notably, the Schild-slopes of both long and short RT antagonists (27 and 5) were close to unity (0.9 ± 0.2 for 27, 1.0 ± 0.2 for 5, Table 4). In addition, the pA₂ value of 5 was comparable with the result from the preincubation condition (7.2 ± 0.4 vs 6.8 ± 0.4, Table 4), and the pA₂ value of 27 was also in agreement with its pK_i value (8.9 ± 0.3 vs 9.4 ± 0.03).

Kinetic Map. Using the association (*k*_{on}) and dissociation (*k*_{off}) rate constants obtained from competition association experiments (Tables 1–3), a kinetic map (Figure 4) was constructed by plotting these values on the *y*-axis and *x*-axis, respectively. The dashed diagonal parallel lines represent the kinetically derived *K*_D values (*K*_D = *k*_{off}/*k*_{on}). Out of this map, three subgroups emerged. Group A represents compounds that exhibit similar *k*_{off} values but with vastly different *k*_{on} values. As a consequence, a diverse range of *K*_D values was observed. Previous SKR studies have primarily focused on optimizing dissociation rates and RTs for predicting in vivo efficacy and creating a kinetically favorable ligand. Yet recently, there has been greater acknowledgment of the important role that the association rate constants may play in determining the efficacy of a drug as the result of increased rebinding or increased drug–target selectivity.¹⁹ A kinetic map would thus allow for the selection of compounds with appropriate RTs while exploring the role of association rate constants in determining

efficacy by choosing a rapidly or slowly associating compound, i.e., 2 or 31 ((2.8 ± 0.5) × 10⁶ M⁻¹ s⁻¹ vs (1.0 ± 0.1) × 10⁵ M⁻¹ s⁻¹). Group B displays ligands that exhibit a narrow range of affinity (*K*_D: 0.1–1 nM) yet a wide range of *k*_{off} values that result in RTs ranging from 20 to 391 min. This information would have gone unnoticed in a traditional SAFIR hit-to-lead approach and would most likely have led to the selection of high affinity compounds not in possession of a potentially efficacy promoting long residence time. Thus, combining SAFIR with SKR aspects in lead optimization would allow the selection of not only potent but also long RT compounds through the drug development pipeline. Lastly, group C represents compounds that present similar *k*_{on} values but due to differing *k*_{off} values show considerable differences in affinities (*K*_D). This illustrates the differences that were observed in the binding kinetics of the R₁ and R₂ substituents, as group C mainly consists of R₁ substituents (noncyclopropylmethyl substituents), while group A mainly consists of R₂ substituents (cyclopropylmethyl substituents). This difference also suggests a different mode of receptor–ligand interaction during the binding process of the two ligand groups.

Altogether, the construction of a kinetic map allows for a more detailed categorization of compounds' affinities as dictated by their kinetic rate constants. In previous studies, such a separation has explained the different therapeutic effects molecules exhibit highlighting the benefits of such an in-depth analysis.^{35,36}

Given the putative link between RT and clinical efficacy, it may be postulated that the lack of hA₃R antagonists progressing from preclinical trials is due to insufficient selection criteria employed in these initial phases of hA₃R drug screening. As previously reported, hA₃R antagonists are reasoned to be beneficial in the treatment of chronic obstructive pulmonary disease (COPD).³⁷ For this indication, a number of antagonists are available that act at the muscarinic M₃ receptor.³⁸ For these therapeutics, their dosing regime and thus duration of action have been linked to their RT. For example, aclidinium, which requires a twice daily dosing regimen, exhibits a much shorter RT than tiotropium that in turn requires only once daily

dosing.¹⁶ This extended duration of action that enables long-lasting efficacy and practical dosing regimens at the muscarinic M₃ receptor is thought to be a beneficial feature in the treatment of chronic illnesses.^{39,40} As hA₃R antagonists can be used to treat chronic COPD but also a number of other chronic disorders, we could imagine that considering the ligand's kinetic profile early in the drug screening process would reduce the likelihood of failure due to insufficient efficacy in future clinical trials. Perhaps when selecting hA₃R antagonists with a favorable long RT, i.e., group A in the kinetic map, will we see the therapeutic potential of the hA₃R fulfilled.

Computational Studies. Finally, we decided to further investigate the ligand–receptor interactions using a homology model of the adenosine A₃ receptor, based on the crystal structure of the adenosine A_{2A} receptor (PDB 4E1Y).⁴¹ WaterMap calculations were applied to try and explain the variance in kinetic profiles of different ligands by unfavorable hydration.^{42,43}

Antagonist **2** (in black stick representation) was docked in the homology model. As a first step, it was placed inside the transmembrane bundle, with the tricyclic ring system surrounded by TM3, TM6, and EL2. Hydrogen bonding was constrained between the amide-hydrogen (–NH₂, δ⁺) from Asn250^{6,55} and the carbonyl-oxygen (–C=O, δ[−]) at the C⁴-position of the pyrido[2,1-*f*]purine-2,4-dione scaffold (Figure 5, left). To compare differences between the ligands, an “apo” WaterMap of the hA₃ receptor was generated. Hydration sites shown as red and orange spheres represent positions where “unstable” water molecules are found. Antagonist **10** (hexyl-substitution), with comparable k_{off} ($(8.2 \pm 1.3) \times 10^{-5} \text{ s}^{-1}$ vs $(6.0 \pm 1.7) \times 10^{-5} \text{ s}^{-1}$) to **2** but 10-fold slower k_{on} ($(2.3 \pm 1.0) \times 10^5 \text{ M}^{-1} \text{ s}^{-1}$ vs $(2.8 \pm 0.5) \times 10^6 \text{ M}^{-1} \text{ s}^{-1}$), was docked with two different binding modes in the same binding site (Figure 5 upper right, cyan and gray sticks). We found additional unstable waters (8, 11, 22 in Figure 5 upper right) surrounding the lipophilic substituents of the compounds, which could be explained as hindrance when the antagonist is associating with the binding site.

The same WaterMap was used to investigate the kinetic profile of antagonist **31**. Indeed, hydration sites 6, 39, 42, and 45 are proposed to be displaced by the 3,4-dichloro substituent. Thus, both the association and dissociation of **31** were slowed down by these unstable waters. For the association process, the lipophilic 3,4-dichloro moiety has difficulty in approaching the occupied unstable hydration sites ($(1.0 \pm 0.1) \times 10^5 \text{ M}^{-1} \text{ s}^{-1}$, slowest k_{on} in the whole series); the same lipophilic 3,4-dichloro substituent seems to provide more stabilization to the receptor–ligand complex, thus hampering the dissociation process ($(5.3 \pm 1.5) \times 10^{-5} \text{ s}^{-1}$, slowest k_{off} in the whole series). Interestingly, by removing a single chloro atom at either the 3- or 4- position on the benzyl-ring (**30** or **29**), association and dissociation rate constants became faster by approximately 10-fold. Although the differences in their k_{on} and k_{off} values were modest (2–3 fold), the unstable hydration sites may prevent the 4-chloro-substituted antagonist **30** from reaching the hydration sites 6, 39, and 42 that interact with the 3-Cl substituent; consequently, both its association and dissociation rate constants were faster than of the 3-chloro-substituted counterpart **29** (k_{on} , $(3.0 \pm 0.3) \times 10^6 \text{ M}^{-1} \text{ s}^{-1}$ vs $(8.2 \pm 1.3) \times 10^5 \text{ M}^{-1} \text{ s}^{-1}$; k_{off} , $(8.2 \pm 0.2) \times 10^{-4} \text{ s}^{-1}$ vs $(4.7 \pm 0.7) \times 10^{-4} \text{ s}^{-1}$).

CONCLUSIONS

We have demonstrated that, next to affinity, additional knowledge of target binding kinetics is useful for selecting and developing new hA₃R antagonists in the early phase of drug discovery. By introducing proper substituents at the N³ position or the N¹ benzyl ring of a series of pyridopyridinediones, divergences in kinetic profiles were observed, while almost all compounds had high and often similar affinity. Two representative ligands (**5** and **27**) were tested in [³⁵S]GTPγS binding assays, confirming the link between their RTs and their (in)surmountable antagonism. According to these findings, a $k_{\text{on}}-k_{\text{off}}-K_{\text{D}}$ kinetic map was constructed and subsequently the antagonists were divided into three subgroups. Additionally, we also performed a computational modeling study that sheds light on the crucial interactions (including with water molecules) for both the association and dissociation kinetics of this family of antagonists. It should be mentioned that the kinetic parameters were derived at the hA₃R, which may be different in, e.g., rodents used in advanced animal models. Still, this study suggests that favorable long RTs would be a proper indicator in the development of hA₃R antagonists for chronic inflammatory conditions, e.g., COPD.

EXPERIMENTAL SECTION

Chemistry. All solvents and reagents were purchased from commercial sources and were of analytical grade. Distilled water will be referred to as H₂O. TLC analysis was performed to monitor the reactions, using Merck silica gel F₂₅₄ plates. Grace Davison Davisil silica column material (LC60A, 30–200 μm) was used to perform column chromatography. Microwave reactions were performed in an Emrys Optimizer (Biotage AB, formerly Personal Chemistry). ¹H and ¹³C NMR spectra were recorded on a Bruker DMX-400 (400 MHz) spectrometer, using tetramethylsilane as internal standard. Chemical shifts are reported in δ (ppm) and the following abbreviations are used: s, singlet; d, doublet; dd, double doublet; t, triplet; m, multiplet. The analytical purity of the final compounds is 95% or higher and was determined by high-performance liquid chromatography (HPLC) with a Phenomenex Gemini 3 μm C18 110A column (50 mm × 4.6 mm, 3 μm), measuring UV absorbance at 254 nm. The sample preparation and HPLC method was as follows: 0.3–0.6 mg of compound was dissolved in 1 mL of a 1:1:1 mixture of CH₃CN/H₂O/*t*-BuOH and eluted from the column within 15 min at a flow rate of 1.3 mL/min. The elution method was set up as follows: 1–4 min isocratic system of H₂O/CH₃CN/1% TFA in H₂O, 80:10:10; from the fourth min, a gradient was applied from 80:10:10 to 0:90:10 within 9 min, followed by 1 min of equilibration at 0:90:10 and 1 min at 80:10:10. Liquid chromatography–mass spectrometry (LC–MS) analyses were performed using a Thermo Finnigan Surveyor–LCQ Advantage Max LC–MS system and a Gemini C18 Phenomenex column (50 mm × 4.6 mm, 3 μm). The elution method was set up as follows: 1–4 min isocratic system of H₂O/CH₃CN/1% TFA in H₂O, 80:10:10; from the fourth min, a gradient was applied from 80:10:10 to 0:90:10 within 9 min, followed by 1 min of equilibration at 0:90:10 and 1 min at 80:10:10.

1-Benzyl-8-methoxy-1*H*,3*H*-pyrido[2,1-*f*]purine-2,4-dione (5).²⁴ 6-Amino-1-benzyluracil (**4**)²⁵ (10.8 g, 49.7 mmol, 1.00 equiv) was suspended in CH₃CN (370 mL). *N*-Bromosuccinimide (17.7 g, 99.4 mmol, 2.00 equiv) was added to the suspension, and the mixture was heated at 80 °C for 1 h, after which full conversion was shown by TLC (1:9 CH₃OH/CH₂Cl₂ + 3% triethylamine). Subsequently, 4-methoxypyridine (15.1 mL, 149.2 mL, 3.00 equiv) was added and the mixture was heated at 80 °C during 10 h. Full consumption of the bromo intermediate was shown by TLC (1% CH₃OH/CH₂Cl₂). A precipitate was formed overnight at RT, which was collected by filtration and washed with diethyl ether. This yielded the desired compound as a white solid (10.2 g, 31.6 mmol, 64%). ¹H NMR (400 MHz, DMSO-*d*₆) δ: 11.11 (s br, 1H), 8.72 (d, *J* = 7.2 Hz, 1H), 7.39–

7.29 (m, 4H), 7.28–7.22 (m, 2H), 6.91 (dd, $J = 7.2, 2.0$ Hz, 1H), 5.19 (s, 2H), 3.89 (s, 3H) ppm. NMR was according to literature data.²⁴

General Procedure for the Preparation of N³-Substituted 1-Benzyl-8-methoxy-1H,3H-pyrido[2,1-f]purine-2,4-diones (1, 2, 6–22).²⁴ The compounds were synthesized using the procedure described by Priego et al.,²⁴ but 5 equiv of the alkyl halide was used instead of 1.5 equiv and the reaction mixture was heated to 80 °C overnight in all cases. The pure compounds were obtained by silica column chromatography using a mixture of petroleum ether/ethyl acetate (2:1) as eluent, if not otherwise stated.

1-Benzyl-8-methoxy-3-propyl-1H,3H-pyrido[2,1-f]purine-2,4-dione (1).²⁴ The pure product was obtained by column chromatography using petroleum ether/ethyl acetate (1:1) as eluent, yielding a white solid 113 mg, 0.31 mmol, 60%. ¹H NMR (400 MHz, CDCl₃) δ : 8.83 (d, $J = 7.2$ Hz, 1H), 7.54 (d, $J = 7.2$ Hz, 2H), 7.34–7.25 (m, 3H), 6.98 (d, $J = 2.0$ Hz, 1H), 6.74 (dd, $J = 7.6, 2.8$ Hz, 1H), 5.37 (s, 2H), 4.02 (t, $J = 7.6$ Hz, 2H), 3.92 (s, 3H), 1.74 (sextet, $J = 7.6$ Hz, 2H), 0.99 (t, $J = 7.6$ Hz, 3H) ppm. MS [ESI + H]⁺: calcd for C₂₀H₂₀N₄O₃, 364.15; found, 365.0.

1-Benzyl-3-(cyclopropylmethyl)-8-methoxy-pyrido[2,1-f]purine-2,4(1H,3H)-dione (2).²³ The pure product was obtained by column chromatography using a mixture of 2% CH₃OH/CH₂Cl₂ as eluent, yielding a white solid, 1.51 g, 3.98 mmol, 86%. ¹H NMR (400 MHz, CDCl₃) δ : 8.82 (d, $J = 7.2$ Hz, 1H), 7.54 (d, $J = 7.2$ Hz, 2H), 7.33–7.23 (m, 3H), 6.97 (d, $J = 2.4$ Hz, 1H), 6.73 (dd, $J = 8.4, 2.4$ Hz, 1H), 5.37 (s, 2H), 3.94 (d, $J = 7.4$ Hz, 2H), 3.92 (s, 3H), 1.35–1.25 (m, 1H), 0.47–0.44 (m, 4H) ppm. MS [ESI + H]⁺: calcd for C₂₁H₂₀N₄O₃, 376.15; found, 376.9.

1-Benzyl-8-methoxy-3-methylpyrido[2,1-f]purine-2,4(1H,3H)-dione (6). Reaction was performed in a sealed tube, and 50 equiv of methyl iodide was used. The residue was purified by silica column chromatography eluting with a petroleum ether/ethyl acetate (1:1) mixture, yielding a white solid, 25 mg, 0.074 mmol, 15%. ¹H NMR (400 MHz, CDCl₃) δ : 8.83 (d, $J = 7.6$ Hz, 1H), 7.54 (d, $J = 7.2$ Hz, 2H), 7.33–7.24 (m, 3H), 6.99 (d, $J = 2.4$ Hz, 1H), 6.75 (dd, $J = 7.6, 2.4$ Hz, 1H), 5.37 (s, 2H), 3.93 (s, 3H), 3.45 (s, 3H) ppm. MS [ESI + H]⁺: calcd for C₁₈H₁₆N₄O₃, 336.12; found, 337.2.

1-Benzyl-3-ethyl-8-methoxy-pyrido[2,1-f]purine-2,4(1H,3H)-dione (7). The pure product was obtained by column chromatography using petroleum ether/ethyl acetate (1:1) as eluent, yielding a white solid, 58 mg, 0.17 mmol, 33%. ¹H NMR (400 MHz, CDCl₃) δ : 8.83 (d, $J = 7.2$ Hz, 1H), 7.54 (d, $J = 7.2$ Hz, 2H), 7.33–7.24 (m, 3H), 6.98 (d, $J = 2.0$ Hz, 1H), 6.74 (dd, $J = 7.6, 2.8$ Hz, 1H), 5.36 (s, 2H), 4.12 (q, $J = 7.2$ Hz, 2H), 3.92 (s, 3H), 1.28 (t, $J = 7.2$ Hz, 3H) ppm. MS [ESI + H]⁺: calcd for C₁₉H₁₈N₄O₃, 350.14; found, 351.0.

1-Benzyl-3-butyl-8-methoxy-pyrido[2,1-f]purine-2,4(1H,3H)-dione (8). Purified by column chromatography using petroleum ether/EtOAc (3:1), yielding a white solid 10 mg, 0.026 mmol, 5%. ¹H NMR (400 MHz, CDCl₃) δ : 8.83 (d, $J = 7.6$ Hz, 1H), 7.54 (d, $J = 6.8$ Hz, 2H), 7.24–7.33 (m, 3H), 6.98 (d, $J = 2.4$ Hz, 1H), 6.74 (dd, $J = 7.4, 2.6$ Hz, 1H), 5.36 (s, 2H), 4.04 (t, $J = 7.6$ Hz, 2H), 3.93 (s, 3H), 1.70–1.64 (m, 2H), 1.40 (sextet, $J = 3.6$ Hz, 2H), 0.95 (t, $J = 7.2$ Hz, 3H) ppm. MS [ESI + H]⁺: calcd for C₂₁H₂₂N₄O₃, 378.17; found, 378.9.

1-Benzyl-8-methoxy-3-pentyl-1H,3H-pyrido[2,1-f]purine-2,4-dione (9). White solid, 110 mg, 0.28 mmol, yield 56%. ¹H NMR (400 MHz, CDCl₃) δ : 8.83 (d, $J = 7.6$ Hz, 1H), 7.56 (d, $J = 7.2$ Hz, 2H), 7.34–7.25 (m, 3H), 6.97 (d, $J = 2.0$ Hz, 1H), 6.74 (dd, $J = 7.6, 2.8$ Hz, 1H), 5.37 (s, 2H), 4.05 (t, $J = 7.6$ Hz, 2H), 3.93 (s, 3H), 1.72–1.66 (m, 2H), 1.39–1.37 (m, 4H), 0.91 (t, $J = 7.2$ Hz, 3H) ppm. MS [ESI + H]⁺: calcd for C₂₂H₂₄N₄O₃, 392.18; found, 393.1.

1-Benzyl-3-hexyl-8-methoxy-pyrido[2,1-f]purine-2,4(1H,3H)-dione (10). White solid, 90 mg, 0.22 mmol, yield 44%. ¹H NMR (400 MHz, CDCl₃) δ : 8.83 (d, $J = 7.2$ Hz, 1H), 7.55 (d, $J = 6.8$ Hz, 2H), 7.34–7.25 (m, 3H), 6.98 (d, $J = 2.0$ Hz, 1H), 6.74 (dd, $J = 7.6, 2.4$ Hz, 1H), 5.37 (s, 2H), 4.05 (t, $J = 7.6$ Hz, 2H), 3.92 (s, 3H), 1.69 (pentet, $J = 7.6$ Hz, 2H), 1.40–1.26 (m, 6H), 0.89 (t, $J = 7.2$ Hz, 3H) ppm. MS [ESI + H]⁺: calcd for C₂₃H₂₆N₄O₃, 406.20; found, 407.1.

1-Benzyl-3-heptyl-8-methoxy-pyrido[2,1-f]purine-2,4(1H,3H)-dione (11). Column chromatography using a mixture of petroleum ether/ethyl acetate (3:1) as eluent yielded 131 mg of the pure product as white solid, 0.31 mmol, 62%. ¹H NMR (400 MHz, CDCl₃) ¹H

NMR (400 MHz, CDCl₃) δ : 8.80 (d, $J = 7.6$ Hz, 1H), 7.54 (d, $J = 6.8$ Hz, 2H), 7.32–7.25 (m, 3H), 6.95 (d, $J = 2.4$ Hz, 1H), 6.71 (dd, $J = 7.2, 2.4$ Hz, 1H), 5.35 (s, 2H), 4.03 (t, $J = 7.6, 2H$), 3.90 (s, 3H), 1.67 (pentet, $J = 7.6$ Hz, 2H), 1.38–1.26 (m, 8H), 0.87 (t, $J = 7.2$ Hz, 3H) ppm. MS [ESI + H]⁺: calcd for C₂₄H₂₈N₄O₃, 420.22; found, 421.2.

3-Allyl-1-benzyl-8-methoxy-pyrido[2,1-f]purine-2,4(1H,3H)-dione (12). Purified by column chromatography using petroleum ether/ethyl acetate (1:1) as eluent, yielding a white solid, 73 mg, 0.20 mmol, 40%. ¹H NMR (400 MHz, CDCl₃) δ : 8.82 (d, $J = 7.6$ Hz, 1H), 7.55 (d, $J = 7.2$ Hz, 2H), 7.34–7.25 (m, 3H), 6.99 (d, $J = 2.0$ Hz, 1H), 6.75 (dd, $J = 7.6, 2.4$ Hz, 1H), 6.02–5.92 (m, 1H), 5.38 (s, 2H), 5.29 (dd, $J = 17.2, 1.2$ Hz, 1H), 5.20 (d, $J = 10.0$ Hz, 1H), 4.68 (d, $J = 5.6$ Hz, 2H), 3.93 (s, 3H) ppm. MS [ESI + H]⁺: calcd for C₂₀H₁₈N₄O₃, 362.14; found, 363.0.

1-Benzyl-8-methoxy-3-(prop-2-yn-1-yl)pyrido[2,1-f]purine-2,4-(1H,3H)-dione (13). The pure product was obtained by column chromatography using petroleum ether/ethyl acetate (1:1) as eluent, yielding a white solid, 60 mg, 0.17 mmol, 3%. ¹H NMR (400 MHz, CDCl₃) δ : 8.82 (d, $J = 7.2$ Hz, 1H), 7.57 (d, $J = 6.8$ Hz, 2H), 7.36–7.26 (m, 3H), 6.99 (d, $J = 2.4$ Hz, 1H), 6.76 (dd, $J = 7.2, 2.4$ Hz, 1H), 5.38 (s, 2H), 4.83 (d, $J = 2.4$ Hz, 2H), 3.94 (s, 3H), 2.19 (t, $J = 2.4$ Hz, 1H) ppm. MS [ESI + H]⁺: calcd for C₂₀H₁₆N₄O₃, 360.12; found, 361.1.

1-Benzyl-3-(but-3-en-1-yl)-8-methoxy-pyrido[2,1-f]purine-2,4-(1H,3H)-dione (14). White solid, 18 mg, 0.05 mmol, yield 10%. ¹H NMR (400 MHz, CDCl₃) δ : 8.84 (d, $J = 7.6$ Hz, 1H), 7.54 (d, $J = 7.2$ Hz, 2H), 7.35–7.28 (m, 3H), 7.00 (d, $J = 2.4$ Hz, 1H), 6.77 (dd, $J = 7.6, 2.4$ Hz, 1H), 5.91–5.84 (m, 1H), 5.39 (s, 2H), 5.08 (dd, $J = 16.8, 1.2$ Hz, 1H), 5.02 (d, $J = 10.4, 1H$), 4.15 (t, $J = 7.2$ Hz, 2H), 3.95 (s, 3H), 2.48 (q, $J = 7.2$ Hz, 2H) ppm. MS [ESI + H]⁺: calcd for C₂₁H₂₀N₄O₃, 376.15; found, 376.9.

1-Benzyl-8-methoxy-3-(2-methoxyethyl)-1H,3H-pyrido[2,1-f]purine-2,4-dione (15). Purified by column chromatography using a mixture of 2% CH₃OH in CH₂Cl₂ yielded the product as a white solid, 70 mg, 0.18 mmol, 37%. ¹H NMR (400 MHz, CDCl₃) δ : 8.83 (d, $J = 7.2$ Hz, 1H), 7.54 (d, $J = 6.8$ Hz, 2H), 7.33–7.24 (m, 3H), 6.98 (d, $J = 2.4$ Hz, 1H), 6.74 (dd, $J = 7.6, 2.4$ Hz, 1H), 5.36 (s, 2H), 4.30 (t, $J = 6.0$ Hz, 2H), 3.93 (s, 3H), 3.68 (t, $J = 6.0$ Hz, 2H), 3.36 (s, 3H) ppm. MS [ESI + H]⁺: calcd for C₂₀H₂₀N₄O₃, 380.15; found, 380.8.

1-Benzyl-3-(3-hydroxypropyl)-8-methoxy-pyrido[2,1-f]purine-2,4-(1H,3H)-dione (16). Purified by column chromatography using a mixture of petroleum ether/EtOAc (1:2), followed by recrystallization from CH₃OH/EtOAc. Yield: white solid, 106 mg, 0.28 mmol, 28%. ¹H NMR (400 MHz, CDCl₃) δ : 8.80 (d, $J = 7.2$ Hz, 1H), 7.53 (d, $J = 7.6$ Hz, 2H), 7.33–7.24 (m, 3H), 6.99 (d, $J = 2.4$ Hz, 1H), 6.76 (dd, $J = 7.6, 2.4$ Hz, 1H), 5.37 (s, 2H), 4.22 (t, $J = 6.0$ Hz, 2H), 3.93 (s, 3H), 3.53 (t, $J = 5.6$ Hz, 2H), 1.92 (pentet, $J = 5.6$ Hz, 2H) ppm. MS [ESI + H]⁺: calcd for C₂₀H₂₀N₄O₃, 380.15; found, 380.9.

1-Benzyl-3-isobutyl-8-methoxy-pyrido[2,1-f]purine-2,4(1H,3H)-dione (17). White solid, 0.08 mmol, 29 mg, yield 15%. ¹H NMR (400 MHz, CDCl₃) δ : 8.86 (d, $J = 7.2$ Hz, 1H), 7.55 (d, $J = 7.2$ Hz, 2H), 7.33–7.28 (m, 3H), 7.00 (d, $J = 2.0$ Hz, 1H), 6.76 (dd, $J = 7.6, 2.4$ Hz, 1H), 5.39 (s, 2H), 3.95 (s, 3H), 3.92 (d, $J = 7.6$ Hz, 2H), 2.22 (nonet, $J = 7.2$ Hz, 1H), 0.97 (d, $J = 6.8$ Hz, 6H) ppm. MS [ESI + H]⁺: calcd for C₂₁H₂₂N₄O₃, 378.17; found, 379.0.

1-Benzyl-8-methoxy-3-(3-neopentyl)-1H,3H-pyrido[2,1-f]purine-2,4-dione (18). Purified by column chromatography using a mixture of 1% CH₃OH in CH₂Cl₂ as eluent, yielding the product as a white solid, 0.025 mmol, 20 mg, 5%. ¹H NMR (400 MHz, CDCl₃) δ : 8.84 (d, $J = 7.2$ Hz, 1H), 7.52 (d, $J = 7.2$ Hz, 2H), 7.32–7.25 (m, 3H), 6.98 (d, $J = 2.4$ Hz, 1H), 6.73 (dd, $J = 7.2, 2.4$ Hz, 1H), 5.37 (s, 2H), 3.99 (s, 2H), 3.92 (s, 3H), 0.98 (s, 9H) ppm. MS [ESI + H]⁺: calcd for C₂₂H₂₄N₄O₃, 392.18; found, 393.0.

1-Benzyl-3-isopentyl-8-methoxy-pyrido[2,1-f]purine-2,4(1H,3H)-dione (19). Yield: white solid, 104 mg, 0.26 mmol, 53%. ¹H NMR (400 MHz, CDCl₃) δ : 8.83 (d, $J = 7.2$ Hz, 1H), 7.53 (d, $J = 7.2$ Hz, 2H), 7.33–7.24 (m, 3H), 6.98 (d, $J = 2.4$ Hz, 1H), 6.74 (dd, $J = 7.6, 2.4$ Hz, 1H), 5.36 (s, 2H), 4.08–4.04 (m, 2H), 3.93 (s, 3H), 1.69 (nonet, $J = 6.8$ Hz, 1H), 1.59–1.53 (m, 2H), 0.98 (d, $J = 6.4$ Hz, 6H) ppm. MS [ESI + H]⁺: calcd for C₂₂H₂₄N₄O₃, 392.18; found, 393.1.

1-Benzyl-3-(3,3-dimethylbutyl)-8-methoxy-pyrido[2,1-*f*]purine-2,4(1*H*,3*H*)-dione (20). Yield: white solid, 81 mg, 0.20 mmol, 40%. ¹H NMR (400 MHz, CDCl₃) δ: 8.84 (d, *J* = 7.6 Hz, 1H), 7.55 (d, *J* = 7.2, 2H), 7.35–7.27 (m, 3H), 6.98 (d, *J* = 2.4 Hz, 1H), 6.74 (dd, *J* = 7.2, 2.4 Hz, 1H), 5.38 (s, 2H), 4.12–4.08 (m, 2H), 3.93 (s, 3H), 1.61–1.57 (m, 2H), 1.04 (s, 9H) ppm. MS [ESI + H]⁺: calcd for C₂₃H₂₆N₄O₃, 406.20; found, 407.1.

1-Benzyl-8-methoxy-3-((trimethylsilyl)methyl)pyrido[2,1-*f*]purine-2,4(1*H*,3*H*)-dione (21). White solid, 137 mg, 0.34 mmol, yield 67%. ¹H NMR (400 MHz, CDCl₃) δ: 8.84 (d, *J* = 7.2 Hz, 1H), 7.50 (d, *J* = 6.8 Hz, 2H), 7.32–7.24 (m, 3H), 6.98 (d, *J* = 2.4 Hz, 1H), 6.73 (d, *J* = 7.2, 2.4 Hz, 1H), 5.39 (s, 2H), 3.93 (s, 3H), 3.64 (s, 2H), 0.08 (s, 9H) ppm. MS [ESI + H]⁺: calcd for C₂₁H₂₄N₄O₃Si, 408.16; found, 409.2.

1-Benzyl-3-(cyclobutylmethyl)-8-methoxy-pyrido[2,1-*f*]purine-2,4(1*H*,3*H*)-dione (22). White solid, 90 mg, 0.23 mmol, yield 46%. ¹H NMR (400 MHz, CDCl₃) δ: 8.82 (d, *J* = 7.2 Hz, 1H), 7.53 (d, *J* = 7.2 Hz, 2H), 7.33–7.13 (m, 3H), 6.69 (d, *J* = 1.8 Hz, 1H), 6.73 (dd, *J* = 7.2, 2.4 Hz, 1H), 5.35 (s, 2H), 4.11 (d, *J* = 7.6 Hz, 2H), 3.92 (s, 3H), 2.83–2.72 (m, 1H), 2.05–1.95 (m, 2H), 1.90–1.79 (m, 4H) ppm. MS [ESI + H]⁺: calcd for C₂₂H₂₂N₄O₃, 390.17; found, 391.2.

3-(Cyclopropylmethyl)-8-methoxy-pyrido[2,1-*f*]purine-2,4(1*H*,3*H*)-dione (23).²³ Prepared following a slightly modified procedure described by Priego et al. In total, four portions of 8 equiv of ammonium formate (after 0, 2, 4, and 6 h) and three portions of 0.15 equiv of 20% Pd(OH)₂ (0, 4, and 6 h) were added, after which full conversion was reached after overnight reflux visualized by TLC (3% CH₃OH/CH₂Cl₂). The reaction mixture was filtered over Celite and the residue extracted 5 times with hot DMF. The combined organic layer was concentrated in vacuo, which resulted in a quantitative yield. ¹H NMR in accordance to data in literature.²³

General Procedure for the Preparation of *N*¹-Substituted-3-cyclopropylmethyl-8-methoxy-1*H*,3*H*-pyrido[2,1-*f*]purine-2,4-diones (24–33).²³ The compounds were synthesized according to the procedure described by Priego et al.² Purification by silica column chromatography using an eluent mixture of petroleum ether/ethyl acetate (3:1) yielded the pure final products.

3-(Cyclopropylmethyl)-8-methoxy-1-(3-methylbenzyl)pyrido[2,1-*f*]purine-2,4(1*H*,3*H*)-dione (24). White solid, 79 mg, 0.20 mmol, yield 57%. ¹H NMR (400 MHz, CDCl₃) δ: 8.84 (d, *J* = 7.2 Hz, 1H), 7.36 (s, 2H), 7.22 (t, *J* = 7.6 Hz, 1H), 7.09 (d, *J* = 7.6 Hz, 1H), 6.99 (d, *J* = 2.4 Hz, 1H), 6.75 (dd, *J* = 7.2, 2.4 Hz, 1H), 5.36 (s, 2H), 3.97 (d, *J* = 7.2 Hz, 2H), 3.94 (s, 3H), 2.34 (s, 3H), 1.37–1.31 (m, 1H), 0.52–0.45 (m, 4H) ppm. MS [ESI + H]⁺: calcd for C₂₂H₂₂N₄O₃, 390.17; found, 391.0.

3-(Cyclopropylmethyl)-8-methoxy-1-(4-methylbenzyl)pyrido[2,1-*f*]purine-2,4(1*H*,3*H*)-dione (25). See ref 23.

3-(Cyclopropylmethyl)-1-(4-ethylbenzyl)-8-methoxy-pyrido[2,1-*f*]purine-2,4(1*H*,3*H*)-dione (26). White solid, 43 mg, 0.11 mmol, yield 21%. ¹H NMR (400 MHz, CDCl₃) δ: 8.82 (d, *J* = 7.6 Hz, 1H), 7.48 (d, *J* = 8.0 Hz, 2H), 7.14 (d, *J* = 8.0 Hz, 2H), 6.98 (d, *J* = 2.0 Hz, 1H), 6.73 (dd, *J* = 7.2, 2.4 Hz, 1H), 5.34 (s, 2H), 3.95–3.93 (m, 5H), 2.60 (q, *J* = 7.6 Hz, 2H), 1.34–1.28 (m, 1H), 1.19 (t, *J* = 7.6 Hz, 3H), 0.50–0.42 (m, 4H) ppm. MS [ESI + H]⁺: calcd for C₂₃H₂₄N₄O₃, 404.18; found, 405.2.

3-(Cyclopropylmethyl)-8-methoxy-1-(3-methoxybenzyl)pyrido[2,1-*f*]purine-2,4(1*H*,3*H*)-dione (27). White solid, 20 mg, 0.049 mmol, yield 14%. ¹H NMR (400 MHz, CDCl₃) δ: 8.83 (d, *J* = 7.6 Hz, 1H), 7.23 (t, *J* = 8.0 Hz, 1H), 7.15–7.10 (m, 2H), 6.97 (d, *J* = 1.6 Hz, 1H), 6.80 (dd, *J* = 8.4, 2.4 Hz, 1H), 6.74 (dd, *J* = 7.6, 2.4 Hz, 1H), 5.35 (s, 2H), 3.96–3.92 (m, 5H), 3.77 (s, 3H), 1.35–1.28 (m, 1H), 0.50–0.45 (m, 4H) ppm. MS [ESI + H]⁺: calcd for C₂₂H₂₂N₄O₄, 406.16; found, 406.9.

3-(Cyclopropylmethyl)-8-methoxy-1-(4-methoxybenzyl)pyrido[2,1-*f*]purine-2,4(1*H*,3*H*)-dione (28). See ref 23.

1-(3-Chlorobenzyl)-3-(cyclopropylmethyl)-8-methoxy-pyrido[2,1-*f*]purine-2,4(1*H*,3*H*)-dione (29). See ref 23.

1-(4-Chlorobenzyl)-3-(cyclopropylmethyl)-8-methoxy-pyrido[2,1-*f*]purine-2,4(1*H*,3*H*)-dione (30). See ref 23.

3-(Cyclopropylmethyl)-1-(3,4-dichlorobenzyl)-8-methoxy-pyrido[2,1-*f*]purine-2,4(1*H*,3*H*)-dione (31). See ref 23.

1-(4-Bromobenzyl)-3-(cyclopropylmethyl)-8-methoxy-pyrido[2,1-*f*]purine-2,4(1*H*,3*H*)-dione (32). White solid, 22 mg, 0.048 mmol, yield 14%. ¹H NMR (400 MHz, CDCl₃) δ: 8.85 (d, *J* = 7.2 Hz, 1H), 7.46 (s, 4H), 6.99 (d, *J* = 1.6 Hz, 1H), 6.87 (dd, *J* = 7.2, 2.0 Hz, 1H), 5.33 (s, 2H), 3.99–3.85 (m, 5H), 1.34–1.24 (m, 1H), 0.50–0.44 (m, 4H) ppm. MS [ESI + H]⁺: calcd for C₂₁H₁₉N₄O₃, 454.06; found, 455.0.

3-(Cyclopropylmethyl)-8-methoxy-1-phenylethylpyrido[2,1-*f*]purine-2,4(1*H*,3*H*)-dione (33). White solid, 112 mg, 0.29 mmol, yield 82%. ¹H NMR (400 MHz, CDCl₃) δ: 8.81 (d, *J* = 7.2 Hz, 1H), 7.35–7.25 (m, 4H), 7.20 (t, *J* = 7.2 Hz, 1H), 6.96 (d, *J* = 2.4 Hz, 1H), 6.73 (dd, *J* = 7.2, 2.4 Hz, 1H), 4.40 (t, *J* = 8.0 Hz, 2H), 3.95–3.90 (m, 5H), 3.12 (t, *J* = 8.0 Hz, 2H), 1.32–1.23 (m, 1H), 0.49–0.40 (m, 4H) ppm. MS [ESI + H]⁺: calcd for C₂₂H₂₂N₄O₃, 390.17; found, 391.0.

Biology. Chemicals and Reagents. [³H]-8-Ethyl-4-methyl-2-phenyl-(8*R*)-4,5,7,8-tetrahydro-1*H*-imidazo[2,1-*i*]-purin-5-one²⁶ ([³H]34, specific activity 56 Ci·mmol⁻¹) was a gift from Prof. C. E. Müller (University of Bonn, Germany). Unlabeled 34 was purchased from Tocris Ltd. (Abingdon, UK). 5'-*N*-Ethylcarboxamidoadenosine (NECA) was purchased from Sigma-Aldrich (Steinheim, Germany). Adenosine deaminase (ADA) was purchased from Boehringer Mannheim (Mannheim, Germany). Bicinchoninic acid (BCA) and BCA protein assay reagents were purchased from Pierce Chemical Company (Rockford, IL, USA). Chinese hamster ovary cells stably expressing the human adenosine A₃ receptor (CHOA₃) were a gift from Dr. K.-N. Klotz (University of Würzburg, Germany). All other chemicals were obtained from standard commercial sources and were of analytical grade.

Cell Culture and Membrane Preparation. Chinese hamster ovary (CHO) cells, stably expressing the human adenosine A₃ receptor (CHOA₃), were cultured and membranes were prepared and stored as previously described.⁴⁴ Protein determination was done through use of the bicinchoninic acid (BCA) method.⁴⁵

Radioligand Displacement Assay. Membrane aliquots containing ~15 μg of CHOA₃ protein were incubated in a total volume of 100 μL of assay buffer (50 mM Tris-HCl, 5 mM MgCl₂, supplemented with 0.01% CHAPS and 1 mM EDTA, pH 7.4) at 25 °C for 120 min. Displacement experiments were performed using six concentrations of competing antagonist in the presence of a final concentration of ~10 nM [³H] 34. At this concentration, total radioligand binding did not exceed 10% of that added to prevent ligand depletion. Nonspecific binding (NSB) was determined in the presence of 100 μM NECA. Incubation was terminated by rapid filtration performed on 96-well GF/B filter plates (PerkinElmer, Groningen, The Netherlands), using a PerkinElmer Filtermate harvester (PerkinElmer, Groningen, The Netherlands). After drying the filter plate at 50 °C for 30 min, the filter-bound radioactivity was determined by scintillation spectrometry using the 2450 MicroBeta³ plate counter (PerkinElmer, Boston, MA).

Radioligand Association and Dissociation Assays. Association experiments were performed by incubating membrane aliquots containing ~15 μg of CHOA₃ membrane in a total volume of 100 μL of assay buffer at 10 or 25 °C with ~10 nM [³H] 34. The amount of radioligand bound to the receptor was measured at different time intervals during a total incubation of 120 min. Dissociation experiments were performed by preincubating membrane aliquots containing ~15 μg of protein in a total volume of 100 μL of assay buffer at 10 or 25 °C for 60 min. After the preincubation, radioligand dissociation was initiated by the addition of 5 μL of 100 μM unlabeled NECA. The amount of radioligand still bound to the receptor was measured at various time intervals for a total of 120 min to ensure that full dissociation from hA₃ receptor was reached. Incubations were terminated and samples were obtained as described under Radioligand Displacement Assay.

Radioligand Competition Association Assay. The binding kinetics of unlabeled ligands were quantified using the competition association assay based on the theoretical framework by Motulsky and Mahan.⁴⁶ The competition association assay was initiated by adding membrane aliquots (15 μg/well) at different time points for a total of 240 min to a total volume of 100 μL of assay buffer at 10 or 25 °C with ~10 nM [³H] 34 in the absence or presence of a single concentration of

competing hA₃R antagonists (i.e., at their IC₅₀ value). Incubations were terminated and samples were obtained as described under **Radioligand Displacement Assay**. The “dual-point” competition association assays were designed as described previously,²⁷ where in this case the two time points were selected at 20 (t₁) and 240 min (t₂).

[³⁵S] GTPγS Binding Assay. The assays were performed by incubating 15 μg of homogenized CHO_hA₃ membranes in a total volume of 80 μL of assay buffer (50 mM Tris-HCl buffer, 5 mM MgCl₂, 1 mM EDTA, 0.05% BSA, and 1 mM DTT, pH 7.4) supplemented with 1 μM GDP and 5 μg of saponin. The assays were performed in a 96-well plate format, where DMSO stock solutions of the compounds were added using a HP D300 Digital Dispenser (Tecan, Männedorf, Switzerland). The final concentration of organic solvent per assay point was ≤0.1%. In all cases, the basal level of [³⁵S] GTPγS binding was measured in untreated membrane samples, whereas the maximal level of [³⁵S] GTPγS binding was measured by treatment of the membranes with 10 μM 2-Cl-IBMECA. For the insurmountability experiments, membrane preparations were preincubated with or without antagonists (30-, 100-, 300-fold K_i values) for 60 min at 25 °C, prior to the addition of 2-Cl-IBMECA (10 μM to 0.1 nM) and 20 μL of [³⁵S] GTPγS (final concentration ~0.3 nM), after which incubation continued for another 30 min at 25 °C. For the surmountability (control) experiments, antagonists and 2-Cl-IBMECA were coincubated with [³⁵S] GTPγS for 30 min at 25 °C. For all experiments, incubations were terminated and samples were obtained as described under **Radioligand Displacement Assay** by using GF/B filters (Whatman International, Maidstone, UK).

Data Analysis. All experimental data were analyzed using the nonlinear regression curve fitting program GraphPad Prism 6.0 (GraphPad Software, Inc., San Diego, CA). From displacement assays, IC₅₀ values were obtained by nonlinear regression analysis of the displacement curves. The obtained IC₅₀ values were converted into K_i values using the Cheng–Prusoff equation to determine the affinity of the ligands.⁴⁷ The observed association rates (k_{obs}) derived from both assays were obtained by fitting association data using one phase exponential association. The dissociation rates were obtained by fitting dissociation data to a one phase exponential decay model. The k_{obs} values were converted into association rate constants (k_{on}) using the equation k_{on} = (k_{obs} - k_{off})/[L], where [L] is the amount of radioligand used for the association experiments. The association and dissociation rates were used to calculate the kinetic K_D using the equation K_D = k_{off}/k_{on}. Association and dissociation rate constants for unlabeled compounds were calculated by fitting the data into the competition association model using “kinetics of competitive binding”:⁴⁶

$$\begin{aligned}
 K_A &= k_1[L] \cdot 10^{-9} + k_2 \\
 K_B &= k_3[I] \cdot 10^{-9} + k_4 \\
 S &= \sqrt{(K_A - K_B)^2 + 4 \cdot k_1 \cdot k_3 \cdot L \cdot I \cdot 10^{-18}} \\
 K_F &= 0.5(K_A + K_B + S) \\
 K_S &= 0.5(K_A + K_B - S) \\
 Q &= \frac{B_{\max} \cdot k_1 \cdot L \cdot 10^{-9}}{K_F - K_S} \\
 Y &= Q \cdot \left(\frac{k_4 \cdot (K_F - K_S)}{K_F \cdot K_S} + \frac{k_4 - K_F}{K_F} e^{(-K_F \cdot X)} - \frac{k_4 - K_S}{K_S} e^{(-K_S \cdot X)} \right)
 \end{aligned}$$

where k₁ is the k_{on} of the radioligand (M⁻¹ s⁻¹), k₂ is the k_{off} of the radioligand (s⁻¹), L is the radioligand concentration (nM), I is the concentration of the unlabeled competitor (nM), X is the time (s), and Y is the specific binding of the radioligand (DPM). The control curve (without competitor) from competition association assays generates the k₁ value, and the k₂ value was obtained from **Radioligand Association and Dissociation Assays**. With that, the k₃, k₄ and B_{max} can be calculated, where k₃ represents the k_{on} (M⁻¹ s⁻¹) of the unlabeled ligand, k₄ stands for the k_{off} (s⁻¹) of the unlabeled ligand, and B_{max}

equals the total binding (DPM). All competition association data were globally fitted. The residence time (RT, in min) was calculated using the equation RT = 1/(60 × k_{off}), as k_{off} values are expressed in s⁻¹. [³⁵S] GTPγS binding curves were analyzed by nonlinear regression using “log (agonist) vs response-variable slope” to obtain potency, inhibitory potency, or efficacy values of agonists and inverse agonists/antagonists (EC₅₀, IC₅₀ or E_{max}, respectively). In the (in)surmountability assays, Gaddum/Schild EC₅₀ shift equations were used to obtain Schild-slopes and pA₂ values; statistical analysis of two-way ANOVA with Tukey’s post-test was applied. All experimental values obtained are means of at least three independent experiments performed in duplicate, unless stated otherwise. R² and P values were calculated using the GraphPad Prism linear regression analysis function. Log P (log partition coefficient) values were calculated using Chemdraw Professional 15.0 (Cambridge Soft, PerkinElmer, Waltham Mass).

Computational Studies. A ligand optimized homology model of the hA₃R was generated by following a similar approach as has been used before⁴⁸ and using the Maestro software package (Schrodinger Inc., New York). In short: first, different homology models were constructed based on the high resolution crystal structure of the adenosine A_{2A} receptor (PDB 4E1Y)⁴¹ and using a sequence alignment from GPCRDB.^{49,50} In the subsequent steps, we iteratively optimized the model using Prime.^{51–53} During every step, the best model was selected based on enrichment (BEDROC-160.9 and ROC). For this, we used a set of 100 diverse antagonists from ChEMBL⁵⁴ obtained by “Cluster Molecules”.⁵⁵ We matched 50 decoys to every ligand ionization state, using the DUD-e web service.⁵⁶ The final model used here showed excellent enrichment (BEDROC-160.9, 0.55; ROC, 0.80). We introduced a long residence time ligand, **2**, in the putative ligand binding site using Induced fit docking,⁵⁷ with H-bond constraints on Asn250^{6,55}. On the basis of this, we generated a WaterMap^{42,43} of the apo state of the receptor. Other ligands were docked using core-constrained docking (using the core of **2** as constraints). Figures were rendered using PyMol.⁵⁸

■ ASSOCIATED CONTENT

Supporting Information

The Supporting Information is available free of charge on the ACS Publications website at DOI: 10.1021/acs.jmedchem.7b00950.

The binding affinities of short RT antagonist (**5**) and long RT antagonist (**27**) at human adenosine A₁ and A_{2A} receptors, the KRI values of pyrido[2,1-f]purine-2,4-dione derivatives without methoxy-substitution at C-8 position, the comparison with their methoxy-substituted counterparts, and the correlation between pk_{off} and Log P of the compounds (PDF)

Molecular formula strings (CSV)

■ AUTHOR INFORMATION

Corresponding Author

*Phone: + 31-71-527-4651. E-mail: ijzerman@lacdr.leidenuniv.nl.

ORCID

Adriaan P. IJzerman: 0000-0002-1182-2259

Author Contributions

L.X., A.P.IJ., and L.H.H. conceived the study. A.P.IJ. and L.H.H. supervised the project. The chemical synthesis was designed and supervised by J.P.D.V. and performed by B.J.K. and J.P.D.V. The bioassays were supervised by L.H.H. and performed by W.A.C.B., T.T.D., E.P., and L.X. The computational work was performed by E.B.L. The manuscript was written by L.X., W.A.C.B., J.P.D.V., and A.P.IJ.

Notes

The authors declare no competing financial interest.

ACKNOWLEDGMENTS

The research in this study has been performed in the “Kinetics for Drug Discovery (K4DD)” consortium. The K4DD project is supported by the Innovative Medicines Initiative Joint Undertaking (IMI JU) under grant agreement no. 115366, resources of which are composed of financial contribution from the European Union’s Seventh Framework Programme (FP7/2007-2013) and EFPIA companies’ in kind contribution. We thank Prof C. E. Mueller (Bonn University, Germany) for her kind help in obtaining [³H] PSB-11, the radiolabeled probe used in this study. Lizi Xia thanks Dr. Daan van der Es for his assistance in preparing the chemistry section.

ABBREVIATIONS USED

ADA, adenosine deaminase; BCA, bichinchonic acid; BSA, bovine serum albumin; CHAPS, 3-[(3-cholamidopropyl)-dimethylammonio]-1-propanesulfonate; CHO, Chinese hamster ovary; COPD, chronic obstructive pulmonary disease; GTP γ S, guanosine 5'-O-[γ -thio]triphosphate; hA₃R, human adenosine A₃ receptor; K_D, equilibrium dissociation constant of ligand; k_{off}, dissociation rate constant; k_{on}, association rate constant; KRI, kinetic rate index; NECA, 5'-(N-ethylcarboxamide)adenosine; RT, residence time; SA(FI)R, structure–affinity relationships; SKR, structure–kinetics relationships

REFERENCES

- (1) Meyerhof, W.; Müller-Brechlin, R.; Richter, D. Molecular cloning of a novel putative G-protein coupled receptor expressed during rat spermiogenesis. *FEBS Lett.* **1991**, *284*, 155–160.
- (2) Fredholm, B. B.; Ijzerman, A. P.; Jacobson, K. A.; Klotz, K.-N.; Linden, J. International union of pharmacology. XXV. Nomenclature and classification of adenosine receptors. *Pharmacol. Rev.* **2001**, *53*, 527–552.
- (3) Jacobson, K. A.; Gao, Z.-G. Adenosine receptors as therapeutic targets. *Nat. Rev. Drug Discovery* **2006**, *5*, 247–264.
- (4) Gessi, S.; Merighi, S.; Varani, K.; Leung, E.; Mac Lennan, S.; Borea, P. A. The A₃ adenosine receptor: an enigmatic player in cell biology. *Pharmacol. Ther.* **2008**, *117*, 123–140.
- (5) Jacobson, K. A.; Moro, S.; Kim, Y.-C.; Li, A.-H. A₃ adenosine receptors: protective vs. damaging effects identified using novel agonists and antagonists. *Drug Dev. Res.* **1998**, *45*, 113–124.
- (6) Nishat, S.; Khan, L. A.; Ansari, Z. M.; Basir, S. F. Adenosine A₃ receptor: a promising therapeutic target in cardiovascular disease. *Curr. Cardiol. Rev.* **2016**, *12*, 18–26.
- (7) Koscsó, B.; Csóka, B.; Pacher, P.; Haskó, G. Investigational A₃ adenosine receptor targeting agents. *Expert Opin. Invest. Drugs* **2011**, *20*, 757–768.
- (8) Fishman, P.; Bar-Yehuda, S.; Synowitz, M.; Powell, J. D.; Klotz, K. N.; Gessi, S.; Borea, P. A. Adenosine receptors and cancer. *Handb. Exp. Pharmacol.* **2009**, *193*, 399–441.
- (9) Zhou, Y.; Schneider, D. J.; Blackburn, M. R. Adenosine signaling and the regulation of chronic lung disease. *Pharmacol. Ther.* **2009**, *123*, 105–116.
- (10) Wilson, C. N.; Nadeem, A.; Spina, D.; Brown, R.; Page, C. P.; Mustafa, S. J. Adenosine receptors and asthma In *Adenosine Receptors in Health and Disease*; Handbook of Experimental Pharmacology, Vol. 193; Springer: Berlin, Heidelberg, 2009; Vol. 193, pp 329–362, DOI 10.1007/978-3-540-89615-9_11.
- (11) Wilson, C. N. Adenosine receptors and asthma in humans. *Br. J. Pharmacol.* **2008**, *155*, 475–486.
- (12) Borea, P. A.; Varani, K.; Vincenzi, F.; Baraldi, P. G.; Tabrizi, M. A.; Merighi, S.; Gessi, S. The A₃ adenosine receptor: history and perspectives. *Pharmacol. Rev.* **2015**, *67*, 74–102.
- (13) Baraldi, P. G.; Cacciari, B.; Romagnoli, R.; Merighi, S.; Varani, K.; Borea, P. A.; Spalluto, G. A₃ adenosine receptor ligands: history and perspectives. *Med. Res. Rev.* **2000**, *20*, 103–128.
- (14) Baraldi, P. G.; Preti, D.; Borea, P. A.; Varani, K. Medicinal chemistry of A₃ adenosine receptor modulators: pharmacological activities and therapeutic implications. *J. Med. Chem.* **2012**, *55*, 5676–5703.
- (15) Hasko, G.; Linden, J.; Cronstein, B.; Pacher, P. Adenosine receptors: therapeutic aspects for inflammatory and immune diseases. *Nat. Rev. Drug Discovery* **2008**, *7*, 759–770.
- (16) Guo, D.; Hillger, J. M.; Ijzerman, A. P.; Heitman, L. H. Drug-target residence time—a case for G protein-coupled receptors. *Med. Res. Rev.* **2014**, *34*, 856–892.
- (17) Cusack, K. P.; Wang, Y.; Hoemann, M. Z.; Marjanovic, J.; Heym, R. G.; Vasudevan, A. Design strategies to address kinetics of drug binding and residence time. *Bioorg. Med. Chem. Lett.* **2015**, *25*, 2019–2027.
- (18) Copeland, R. A.; Pompliano, D. L.; Meek, T. D. Drug-target residence time and its implications for lead optimization. *Nat. Rev. Drug Discovery* **2006**, *5*, 730–739.
- (19) Copeland, R. A. The drug-target residence time model: a 10-year retrospective. *Nat. Rev. Drug Discovery* **2016**, *15*, 87–95.
- (20) Zeilinger, M.; Pichler, F.; Nics, L.; Wadsak, W.; Spreitzer, H.; Hacker, M.; Mitterhauser, M. New approaches for the reliable in vitro assessment of binding affinity based on high-resolution real-time data acquisition of radioligand-receptor binding kinetics. *EJNMMI Res.* **2017**, *7*, 22.
- (21) Guo, D.; Heitman, L. H.; Ijzerman, A. P. Kinetic aspects of the interaction between ligand and G protein-coupled receptor: the case of the adenosine receptors. *Chem. Rev.* **2017**, *117*, 38–66.
- (22) Topliss, J. G. A manual method for applying the Hansch approach to drug design. *J. Med. Chem.* **1977**, *20*, 463–469.
- (23) Priego, E.-M.; Pérez-Pérez, M.-J.; von Frijtag Drabbe Kuenzel, J. K.; de Vries, H.; Ijzerman, A. P.; Camarasa, M.-J.; Martín-Santamaría, S. Selective human adenosine A₃ antagonists based on pyrido[2,1-f]purine-2,4-diones: novel features of hA₃ antagonist binding. *ChemMedChem* **2008**, *3*, 111–119.
- (24) Priego, E.-M.; von Frijtag Drabbe Kuenzel, J.; Ijzerman, A. P.; Camarasa, M.-J.; Pérez-Pérez, M.-J. Pyrido[2,1-f]purine-2,4-dione derivatives as a novel class of highly potent human A₃ adenosine receptor antagonists. *J. Med. Chem.* **2002**, *45*, 3337–3344.
- (25) Kalla, R.; Perry, T.; Elzein, E.; Varkhedkar, V.; Li, X.; Ibrahim, P.; Palle, V.; Xiao, D.; Zablocki, J. Xanthine Derivatives as A_{2B} Adenosine Receptor Antagonists. WO2004106337 A1, 2004.
- (26) Müller, C. E.; Diekmann, M.; Thorand, M.; Ozola, V. [3H]8-Ethyl-4-methyl-2-phenyl-(8R)-4,5,7,8-tetrahydro-1H-imidazo[2,1-i]purin-5-one ([3H]PSB-11), a novel high-affinity antagonist radioligand for human A₃ adenosine receptors. *Bioorg. Med. Chem. Lett.* **2002**, *12*, 501–503.
- (27) Guo, D.; van Dorp, E. J. H.; Mulder-Krieger, T.; van Veldhoven, J. P. D.; Brussee, J.; Ijzerman, A. P.; Heitman, L. H. Dual-point competition association assay: a fast and high-throughput kinetic screening method for assessing ligand-receptor binding kinetics. *J. Biomol. Screening* **2013**, *18*, 309–320.
- (28) Vauquelin, G. Cell membranes... and how long drugs may exert beneficial pharmacological activity in vivo. *Br. J. Clin. Pharmacol.* **2016**, *82*, 673–682.
- (29) Hu, M.-H.; Chen, X.; Chen, S.-B.; Ou, T.-M.; Yao, M.; Gu, L.-Q.; Huang, Z.-S.; Tan, J.-H. A new application of click chemistry in situ: development of fluorescent probe for specific G-quadruplex topology. *Sci. Rep.* **2015**, *5*, 17202.
- (30) Kolb, H. C.; Sharpless, K. B. The growing impact of click chemistry on drug discovery. *Drug Discovery Today* **2003**, *8*, 1128–1137.

- (31) Tian, H.; Fürstenberg, A.; Huber, T. Labeling and single-molecule methods to monitor G protein-coupled receptor dynamics. *Chem. Rev.* **2017**, *117*, 186–245.
- (32) Tummino, P. J.; Copeland, R. A. Residence time of receptor–ligand complexes and Its Effect on Biological Function. *Biochemistry* **2008**, *47*, 5481–5492.
- (33) Smith, G. F. Medicinal chemistry by the numbers: the physicochemistry, thermodynamics and kinetics of modern drug design. In *Progress in Medicinal Chemistry*; Lawton, G., Witty, D. R., Eds.; Elsevier BV: Burlington, 2009; Vol. 48, p 1.
- (34) Wilcken, R.; Zimmermann, M. O.; Lange, A.; Joerger, A. C.; Boeckler, F. M. Principles and applications of halogen bonding in medicinal chemistry and chemical biology. *J. Med. Chem.* **2013**, *56*, 1363–1388.
- (35) Markgren, P.-O.; Schaal, W.; Hämäläinen, M.; Karlén, A.; Hallberg, A.; Samuelsson, B.; Danielson, U. H. Relationships between structure and interaction kinetics for HIV-1 protease inhibitors. *J. Med. Chem.* **2002**, *45*, 5430–5439.
- (36) Yu, Z.; van Veldhoven, J. P. D.; Louvel, J.; 't Hart, I. M. E.; Rook, M. B.; van der Heyden, M. A. G.; Heitman, L. H.; Ijzerman, A. P. Structure–affinity relationships (SARs) and structure–kinetics relationships (SKRs) of Kv11.1 blockers. *J. Med. Chem.* **2015**, *58*, 5916–5929.
- (37) Polosa, R.; Blackburn, M. R. Adenosine receptors as targets for therapeutic intervention in asthma and chronic obstructive pulmonary disease. *Trends Pharmacol. Sci.* **2009**, *30*, 528–535.
- (38) Barnes, P. J. The role of anticholinergics in chronic obstructive pulmonary disease. *Am. J. Med. Supplements* **2004**, *117*, 24–32.
- (39) Tashkin, D. P. Is a long-acting inhaled bronchodilator the first agent to use in stable chronic obstructive pulmonary disease? *Curr. Opin. Pulm. Med.* **2005**, *11*, 121–128.
- (40) Cazzola, M.; Page, C. Long-acting bronchodilators in COPD: where are we now and where are we going? *Breathe* **2014**, *10*, 110–120.
- (41) Liu, W.; Chun, E.; Thompson, A. A.; Chubukov, P.; Xu, F.; Katritch, V.; Han, G. W.; Roth, C. B.; Heitman, L. H.; Ijzerman, A. P.; Cherezov, V.; Stevens, R. C. Structural basis for allosteric regulation of GPCRs by sodium ions. *Science* **2012**, *337*, 232–236.
- (42) Abel, R.; Young, T.; Farid, R.; Berne, B. J.; Friesner, R. A. Role of the active-site solvent in the thermodynamics of factor Xa ligand binding. *J. Am. Chem. Soc.* **2008**, *130*, 2817–2831.
- (43) Young, T.; Abel, R.; Kim, B.; Berne, B. J.; Friesner, R. A. Motifs for molecular recognition exploiting hydrophobic enclosure in protein–ligand binding. *Proc. Natl. Acad. Sci. U. S. A.* **2007**, *104*, 808–813.
- (44) Heitman, L. H.; Göblyös, A.; Zweemer, A. M.; Bakker, R.; Mulder-Krieger, T.; van Veldhoven, J. P. D.; de Vries, H.; Brussee, J.; Ijzerman, A. P. A Series of 2,4-disubstituted quinolines as a new class of allosteric enhancers of the adenosine A3 receptor. *J. Med. Chem.* **2009**, *52*, 926–931.
- (45) Smith, P. K.; Krohn, R. I.; Hermanson, G. T.; Mallia, A. K.; Gartner, F. H.; Provenzano, M. D.; Fujimoto, E. K.; Goetze, N. M.; Olson, B. J.; Klenk, D. C. Measurement of protein using bicinchoninic acid. *Anal. Biochem.* **1985**, *150*, 76–85.
- (46) Motulsky, H. J.; Mahan, L. C. The kinetics of competitive radioligand binding predicted by the law of mass action. *Mol. Pharmacol.* **1984**, *25*, 1–9.
- (47) Cheng, Y.-C.; Prusoff, W. H. Relationship between the inhibition constant (K_i) and the concentration of inhibitor which causes 50% inhibition (IC_{50}) of an enzymatic reaction. *Biochem. Pharmacol.* **1973**, *22*, 3099–3108.
- (48) Louvel, J.; Guo, D.; Soethoudt, M.; Mocking, T. A.; Lenselink, E. B.; Mulder-Krieger, T.; Heitman, L. H.; Ijzerman, A. P. Structure-kinetics relationships of Capadenoson derivatives as adenosine A1 receptor agonists. *Eur. J. Med. Chem.* **2015**, *101*, 681–691.
- (49) Isberg, V.; Mordalski, S.; Munk, C.; Rataj, K.; Harpsøe, K.; Hauser, A. S.; Vroiling, B.; Bojarski, A. J.; Vriend, G.; Gloriam, D. E. GPCRdb: an information system for G protein-coupled receptors. *Nucleic Acids Res.* **2016**, *44*, D356–D364.
- (50) Munk, C.; Isberg, V.; Mordalski, S.; Harpsøe, K.; Rataj, K.; Hauser, A.; Kolb, P.; Bojarski, A.; Vriend, G.; Gloriam, D. GPCRdb: the G protein-coupled receptor database—an introduction. *Br. J. Pharmacol.* **2016**, *173*, 2195–2207.
- (51) *Schrödinger Release 2016-3 Prime*; Schrödinger LLC: New York, 2016.
- (52) Jacobson, M. P.; Friesner, R. A.; Xiang, Z.; Honig, B. On the role of the crystal environment in determining protein side-chain conformations. *J. Mol. Biol.* **2002**, *320*, 597–608.
- (53) Jacobson, M. P.; Pincus, D. L.; Rapp, C. S.; Day, T. J.; Honig, B.; Shaw, D. E.; Friesner, R. A. A hierarchical approach to all-atom protein loop prediction. *Proteins: Struct., Funct., Genet.* **2004**, *55*, 351–367.
- (54) Gaulton, A.; Bellis, L. J.; Bento, A. P.; Chambers, J.; Davies, M.; Hersey, A.; Light, Y.; McGlinchey, S.; Michalovich, D.; Al-Lazikani, B.; Overington, J. P. ChEMBL: a large-scale bioactivity database for drug discovery. *Nucleic Acids Res.* **2012**, *40*, D1100–D1107.
- (55) *Pipeline Pilot*, version 9.2; Scitegic Accelrys Software Inc.: San Diego, 2016.
- (56) Mysinger, M. M.; Carchia, M.; Irwin, J. J.; Shoichet, B. K. Directory of useful decoys, enhanced (DUD-E): better ligands and decoys for better benchmarking. *J. Med. Chem.* **2012**, *55*, 6582–6594.
- (57) Sherman, W.; Day, T.; Jacobson, M. P.; Friesner, R. A.; Farid, R. Novel procedure for modeling ligand/receptor induced fit effects. *J. Med. Chem.* **2006**, *49*, 534–553.
- (58) *The PyMOL Molecular Graphics System*, version 1.8; Schrödinger, LLC: New York, 2016.